

**FIELD DEPENDENT MAGNETORESISTANCE AND SPIN GLASS
BEHAVIOR OF $\text{Fe}_{73}\text{Cu}_1\text{Nb}_{3.5}\text{Si}_{14}\text{B}_{8.5}$ AMORPHOUS ALLOY**



**BY
VINCENT TITAS ROZARIO
ROLL: 100114022¹P**

**A THESIS SUBMITTED TO THE DEPARTMENT OF PHYSICS OF
BANGLADESH UNIVERSITY OF ENGINEERING AND TECHNOLOGY IN
PARTIAL FULFILMENT OF THE REQUIREMENT FOR THE DEGREE OF
MASTER OF PHILOSOPHY**



**DEPARTMENT OF PHYSICS
BANGLADESH UNIVERSITY OF ENGINEERING AND TECHNOLOGY
DDHAKA, BANGLADESH
SEPTEMBER, 2007**



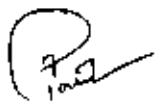
BANGLADESH UNIVERSITY OF ENGINEERING & TECHNOLOGY (BUET)
DHAKA
DEPARTMENT OF PHYSICS

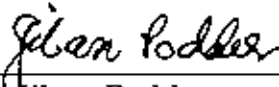



Certification of thesis work

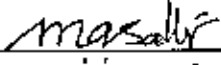
The thesis titled "*FIELD DEPENDENT MAGNETORESISTANCE AND SPIN GLASS BEHAVIOR OF $Fe_{73}Cu_1Nb_{3.5}Si_{14}B_{8.5}$ AMORPHOUS ALLOY*", submitted by VINCENT TITAS ROZARIO, Roll No: 100114022P, Registration No: 0110833, Session: October 2001, has been accepted as satisfactory in partial fulfillment of the requirement for the degree of **MASTER OF PHILOSOPHY (M. Phil.)** in Physics on **29 September, 2007.**

BOARD OF EXAMINERS

1. 

Dr. Md. Feroz Alam Khan (Supervisor) Chairman
Professor, Department of Physics
BUET, Dhaka-1000
2. 

Dr. Jiban Podder Member (Ex-Officio)
Professor & Head
Department of Physics
BUET, Dhaka-1000
3. 

Dr. Md. Mostak Hossain Member
Associate Professor, Department of Physics
BUET, Dhaka-1000
4. 

Dr. Md. Abdus Satter Member (External)
Professor
Department of Physics
University of Dhaka, Dhaka

DECLARATION

This is to certify that the author is solely responsible for the work reported in this thesis and this work has not been submitted to any university or elsewhere for the award of any degree or diploma.

Candidate



(Vincent Titas Rozario)

Roll No: 100114022P

Session : October-2001

DEDICATED
TO
MY BELOVED
PARENTS

ACKNOWLEDGEMENT

I am deeply indebted to my supervisor Dr. Md. Feroz Alam Khan, Professor, Department of Physics, Bangladesh University of Engineering and Technology whose help, stimulating suggestions and encouragement helped me during the course of my research work till writing of this thesis. Throughout my M.Phil research work his encouragement and support has helped me to develop independent thinking and research skills. He continually stimulated my analytical thinking and greatly assisted me with scientific writing.

My grateful acknowledgement to Prof. Dr. Jiban Podder, Head of the department of Physics, BUET, Prof. Dr.Mominul Haq, Prof. Dr.Abu Hashan Bhuiyan, Prof. Dr. Nazma Zaman, Dr.Md. Mostak Hossain and all other respected faculty members and staff of the Physics Department, BUET for their cooperation during the research work.

I am thankful to Bangladesh University of Engineering and Technology (BUET) to provide financial assistance to carry out this research project.

I wish to convey my sincere gratefulness to the principal Rev. Fr. Benjamin Costa CSC, Principal Notre Dame College, Dhaka and to my Notre Dame Family.

I am extremely grateful for the assistance I received from my colleagues Susanta Kumar Sarkar, Dharendra Kumar Ray, Badrul Alam, Habibur Rahaman and Philip Rozario and other staff of Physics Department of Notre Dame College. Their assistance made it possible for me to complete my work.

I extend many thanks to my students and special thanks to Jude and Vaswati for their computer work.

Finally, I'd like to thank my family. I'm grateful to my father and mother for their encouragement and enthusiasm. I'd like to thank my father in law and mother in law also for their encouragement.

I'm especially grateful to my wife and best friend, Chitra, for her patience and for helping me keep my life in proper perspective and balance and was a constant source of support and love to my two little daughters Joyee and Nidhi.

Abstract

$\text{Fe}_{73}\text{Cu}_1\text{Si}_{14}\text{Nb}_{3.5}\text{B}_{8.5}$ magnetic alloy has been prepared in the form of ribbon by single roller melt-spinning technique. In order to study magneto-resistance (MR) and spin glass behavior of the alloy the MR% have been measured in different magnetic field as a function of temperature; ac permeability have been measured at room temperature as a function of frequency to investigate the frequency dependence of permeability. A significant improvement in magnetic properties of this alloy system has been observed upon controlled annealing the sample close to the crystallization temperature. The typical amorphous nature of the as grown alloy is observed by X-Ray diffraction with the appearance of a broad peak over an scanning angular range from 3° to 70° . Magnetization measurements on the as cast and on annealed samples have shown a gradual improvement of magnetic softness upto the highest annealing time and temperature before the boride phase is appeared where the magnetic softness begin to drop. The gradual enhancement of magnetization indicates the onset of nanocrystalline structure. The differential scanning calorimetry (DSC) measurements have been done on the annealed samples to find the formation of nano grains. Field Cool (FC) and Zero Field Cooled (ZFC) measurements have been done to observe some possible relaxation effect. It is observed from these measurements that a small but clear bifurcation in the Magnetization versus Temperature curves has taken place well below the glass transition temperature depicting a spin-glass like behavior.

CONTENTS

	Page No
Content	i
List of Figures	iii
List of Symbols Used	v

Chapter-1

Introduction

1.1 Introduction	1
1.2 Characteristics of Finemet	3
1.3 Importance of Nanocrystalline alloy	5
1.4 Review of this work	5
1.5 Aim of this Work	12

Chapter-2

Theoretical Aspects

2.1 Formation of Nano-crystalline state	13
2.2 Microstructure and effects of grain size	14
2.3 Temperature Dependence of the Magnetic Properties	18
2.4 High Frequency Behavior and Losses	19
2.5 Magnetization of Nano-crystalline Alloys	19
2.6 Electrical Resistivity	21
2.7 Magnetoresistance of the Amorphous Alloys	22
2.8 Spin -Glass behavior of Amorphous alloy	23

Chapter-3

Method of Sample Preparation

3.1 Method of Sample Preparation	25
3.1.1 The Fast Cooling of the Melt	26
3.1.2 Rapid Quenching Method	27
3.2 Important Factors to Control the Thickness of Ribbons	28
3.3 Conditions for the Formation of Nano-crystalline Materials	28
3.4 Resistivity Measurement	30
3.5 I-V Measurement at Room Temperature	31
3.6 I-V Measurement at high Temperature	31
3.7 Magnetoresistance Measurement	35

3.8 Measurement of Magnetisation	35
3.9 Working Principle of Vibrating Sample Magnetometer (VSM)	35
3.9.1 Principle	36
3.10 Permeability Measurement	37
3.10.1 Theory of Permeability	37
3.11 Permeability Measurement	38

Chapter-4

Results and Discussions

4.1. X-ray diffraction	42
4.2 Magnetic permeability	43
4.3 Temperature dependent magnetoresistance	46
4.4 Magnetization Measurements	49
4.5 Differential Scanning Calorimetry (DSC)	51
4.6 Spin-Glass	52

Chapter-5

5.1 Conclusion	54
5.2 Suggestions for future work	55
Bibliography	56-58
Appendix	59-68

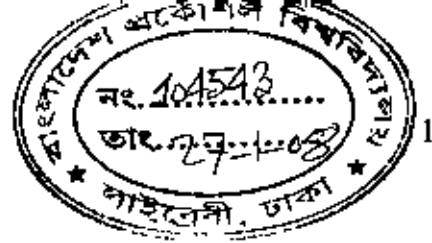
List of the Figures

	Page No
1.2 Relationship between relative permeability and saturation flux density of various soft magnetic materials	3
1.2 Examples of DC B-H Curve	4
2.1 A typical TEM bright field image of $\text{Fe}_{73.5}\text{Si}_{13.5}\text{B}_9\text{Nb}_3\text{Cu}_1$ rapidly solidified alloy. The nanocrystalline bcc phase with an average grain size of ~10nm.	15
2.2 Concentration depth profile of $\text{Fe}_{73.5}\text{Si}_{13.5}\text{B}_9\text{Nb}_3\text{Cu}_1$ alloy annealed at 550°C for 60min. The presence of three types of phases are clearly identified.	15
2.3 Crystallization process of FINEMET	16
2.4 Relationship between crystal grain diameter (D) and coercive force (H_c)	18
3.1 Manufacturing process of "FINEMET"	27
3.2 Four-point probe technique to measure resistivity	30
3.3 The schematic diagram of the experimental setup for I~V measurement at high temperature	32
3.4 Schematic diagram of such a high temperature oven.	34
3.1 I(a) Sample holder structure	40
3.1 I(b) A schematic diagram of Agilent Impedance Analyzer	41
4.1 X-Ray Diffraction	42

4.2.1 Frequency vs. Permeability for As-cast sample	44
4.2.2 Frequency vs. Permeability for As-cast and Annealed Sample	45
4.3.1 Field vs. Magnetoresistance	47
4.3.2 Field vs. Magnetoresistance	48
4.4 Field vs. Magnetization	50
4.5 Differential Scanning Calorimetry	51
4.6 Field cool and Zero field cool	52

List of the Symbol Used

DTA	Differential Thermal Analysis
XRD	X-ray diffraction
VSM	Vibrating Sample Magnetometer
TEM	Transmission Electron Microscope
T_g	Glass Transition Temperature
T_s	Crystallization Temperature
T_a	Annealing Temperature
t_a	Annealing Time
T_c	curic Temperature
K₁	Anisotropy Constant
H_c	Coercive Force
μ	Permeability
μ'	Real Part of the Complex Permeability
μ''	Imaginary Part of the Complex Permeability
B	Magnetic Induction
H	Magnetic Field
χ	Magnetic Susceptibility
a₀	Lattice Parameter
D_g	Grain size
M_s	saturation Magnetization
B_s	Saturation Magnetic Flux Density



Chapter-1: Introduction

1.1 Introduction

The Fe-Cu-Nb-Si-B nanocrystalline alloys are well known because of their excellent soft magnetic properties and this iron based nanocrystalline obtained by crystallization of amorphous alloys were first reported by Yoshizawa in 1988 and known under commercial name as Finemet. Finemet can be prepared by a controlled crystallization of amorphous Fe-Si alloys with additions of Cu-Nb exhibits a very high saturation magnetic flux density, high permeability (of the order of 10^5), low coercive field (below 1 Amp/m), low magnetostriction and this unique soft magnetic material have an enormous potential for applications like energy saving, electromagnetic noise reduction and also great for size reduction. In 1988, Yoshizawa et al. [1, 2] reported that excellent permeability is obtained when the crystal grain size is reduced to a nanometer scale by crystallizing the Fe-Si-B-Nb-Cu amorphous alloy. The principle of magnetic softening accompanied by the reduction of the grain size in the nanoscale range was later explained based on the random anisotropy theory by Herzer [3, 4]. According to this model, the origin of the magnetic softness is ascribed to the reduced magnetocrystalline anisotropy due to the random distribution of nanoscale grains.

The precursor of FINEMET is amorphous ribbon (noncrystalline) obtained by rapid quenching at one million $^{\circ}$ C/second from the molten metal consisting of Fe, Si, B and small amounts of Cu and Nb. Amorphous magnetic metal has high permeability due to no crystalline magnetic anisotropy. Consequently, it has superior soft magnetic characteristics, such as lower core loss, "when compared with conventional crystalline soft magnetic materials". However when applying heat treatment on typical amorphous metal at temperature higher than its crystallization temperature, its magnetic properties will decay tremendously due to rapid crystal growth up to sub μ m ($<1\mu$ m). It was discovered that amorphous metals which contain certain alloy elements show superior soft magnetic properties through crystallization. These crystallized alloys have grains which are extremely uniform and small, "about ten nanometers in size". It was commonly known that

the characteristics of soft magnetic materials are “larger crystal grains yield better soft magnetic properties”. Contrary to this common belief, soft magnetic material consisting of a small, “nano-order”, crystal grains have excellent soft magnetic properties.

The sample $Fe_{73}Cu_1Nb_3Si_{14}B_{8.5}$ is an excellent soft magnetic material due to its random anisotropy effect. This Finemet consisting of ultrafine grain structures prepared by the crystallization of Fe-Si-B amorphous alloys with added Copper and Niobium have the effect of the formation of b.c.c. crystalline nuclei and the suppression of crystal grain growth respectively. This amorphous alloy with nanocrystallites system transform s to the nanocrystalline phase when annealed above the crystallization temperature giving rise to the grain size 10-15 nanometers. However their intrinsic parameters e.g. saturation magnetization M_s and the ferromagnetic transition temperature T_c is not known to have been affected due to this transformation. But their permeability increases substantially and the coercive field becomes too low making this kind of alloy system a very useful magnetic material for the fabrication of magnetic devices and sensors. The magnetostriction constants of this soft magnetic material also approaches to zero as the temperature is increased closed to the transition temperature T_g . Another interesting property of this alloy system is its super paramagnetic behavior at low temperature. With the reduction of particle size from submicron to the nanocrystalline state, the magnetization vectors also take innumerable orientations rather than one single vector for a single domain particle. Annealing this alloy system at a temperature closed to the crystallization temperature causes the iron particles to form local segregation. This isolated iron crytallites interact very weakly with each other according to the Rudermann-Kasuya-Yoshida (RKKY) interaction. Although the interaction between these dispersed particles is of dipole-dipole nature, they show single particle dynamics as well at very low temperature giving rise to the magnetic relaxation effect which is a characteristic feature of spin glass.

1.2 Characteristics of Finemet

1) High saturation magnetic flux density and high permeability

High saturation magnetic flux density comparable to Fe-based amorphous metal. High permeability comparable to Co-based amorphous metal.

Fig. 1 shows relationship between saturation magnetic flux density (B_s) and relative permeability (μ) of various soft magnetic materials, including FINEMET. Soft magnetic materials are usually required to have high flux density and high relative permeability at the same time. In this figure, a material located at upper right position shows better performance as a soft magnetic material. The dotted line represents the magnetic properties limit for the conventional soft magnetic materials, such as ferrite and amorphous metal. FINEMET crosses over this boundary (dotted line), FINEMET has permeability as high as Co-based amorphous metal and a saturation magnetic flux density as high as Fe-based amorphous metal.

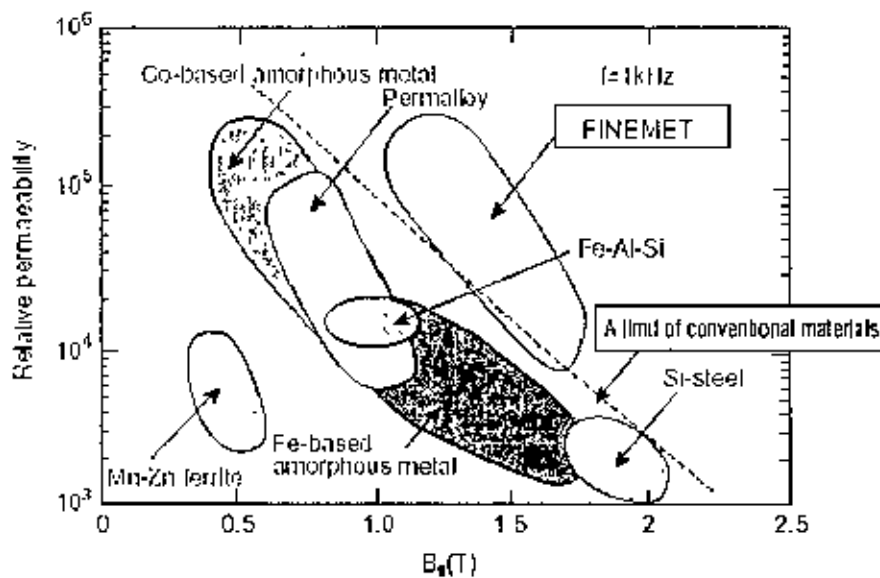


Fig 1 Relationship between relative permeability and saturation flux density of various soft magnetic materials

2) Low core loss

1/5th the core loss of Fe based amorphous metal and approximately the same core loss as Co-based amorphous metal.

3) Low magnetostriction

Less affected by mechanical stress. Very low audio noise emission.

4) Excellent temperature characteristics and small aging effects

Small permeability variation (less than $\pm 10\%$) at a temperature range of -50°C - 150°C . Unlike Co-based amorphous metals, aging effects are very small.

5) Excellent high frequency characteristics (low core loss due to thin ribbon and high electric resistivity)

High permeability and low core loss over wide frequency range, which is equivalent to Co-based amorphous metal.

6) Flexibility to control magnetic properties, "B-H curve shape" during annealing

Three types of B-H curve squareness, high, middle and low remanence ratio, corresponding to various applications.

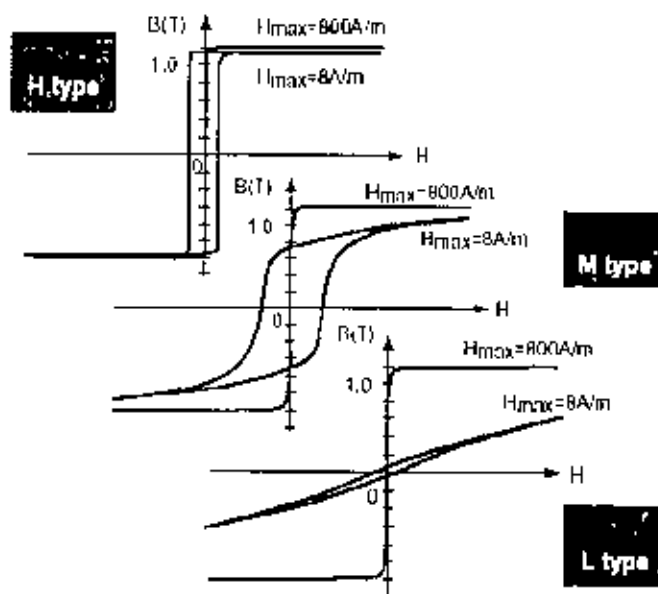


Fig. 2 Examples of DC B-H curve

1.3 Importance of Nanocrystalline alloy

FINEMET has great potential use as core material and can also be used for superior electromagnetic noise suppression for electric and electronic devices. FINEMET has unique magnetic properties which will allow a significant reduction in size and weight of core material and low energy loss which will contribute to energy conservation. The advantages of the unique characteristics of the nanocrystalline alloys can be developed the materials technology and it is the new solution for various applications such as

Magnetic amplifier, Pulse power cores, Surge absorbers, High voltage pulse transformers

Storable cores, EMI filters, Common mode chokes, Magnetic shielding sheets,

Electromagnetic wave absorbers, Current sensors, Magnetic sensors, High frequency power transformers, Active filters, Smoothing choke coils, Accelerator cavity, Energy saving Size/weight reduction, Noise suppression.

1.4 Review of this work

The effects of the metalloid composition and annealing temperature (400 – 720 °C) on the magnetic properties of $Fe_{73.5}Cu_1Nb_3Si_{22.5-x}B_x$ ($x= 5,10$ at %) nanocrystalline alloys has been investigated. Crystallization products were studied using x-ray diffractometry. The coercive field, remanence, and out of ribbon axis anisotropy were determined from quasi static hysteresis loops. It was found that the beginning of nanocrystallization causes some magnetic hardening, which is manifested in a remarkable increase in coercive field for all alloys studied. This effect is ascribed to the increase in magnetostriction. The softest magnetic behavior was observed for alloys with nanocrystalline structure composed of α -Fe (Si), Fe_3Si and an amorphous matrix. The very strong magnetic hardening coincides with the second stage of crystallization and the appearance of Borides (e.g. Fe_2B). The Si-rich alloys also exhibit minor hardening after annealing at temperatures well below the onset temperature of the second stage of crystallization. This effect is attributed to the increase in grain size and the precipitation of copper crystals.

The magnetic softness of these nanocrystalline materials is related to the vanishing magneto-crystalline anisotropy and very small magnetostriction. As was theoretically estimated by Herzer [5], the average anisotropy for randomly oriented α -Fe(Si) grains is negligible small when the grain diameter does not exceed above 15 nm. Such an ultrafine structure can be obtained by a conventional furnace annealing of alloys specific compositions, e.g. Fe-Cu-Nb-Si-B alloys [1, 5, 6, 7, and 8]. It is believed that the magnetostriction constant λ of two phase nanocrystalline materials is determined by the balance between the crystallites ($\lambda_{cr} < 0$) and the amorphous matrix ($\lambda_{am} < 0$) [9]. However, the values of both λ_{cr} and λ_{am} depend on the Si-content. On the other hand, the magnetostriction of nanocrystalline materials depends strongly on the temperature of the nanocrystallization [10, 11]. Therefore the concentrations of silicon and boron, as well as the annealing temperature, are important factors influencing magnetic properties of nanocrystalline Fe-based alloys.

The magnetic softening corresponds to the nanocrystalline structure consisting of α -Fe(Si), Fe₃Si and an amorphous matrix. It was obtained after annealing the alloys at temperatures exceeding the crystallization onset temperature T_{a1} and below the onset temperature T_{a2} of the 2nd stage of crystallization. This softening is a well known result of decreasing magnetostriction and vanishing magneto-crystalline anisotropy and is a practical goal of nanocrystallization. The softest magnetic behavior was found only in the nanocrystalline state for all the alloys studied.

The most striking result of this study is the magnetic hardening 111, which is manifested in the maxima of H_i observed for all the alloys studied after annealing at temperatures slightly exceeding the crystallization onset temperature T_{a1} . This effect can be ascribed to the increase in magnetostriction which also shows a local maximum at the same range of T_{a1} for the alloy containing as % boron. Similar maxima in the saturation magnetostriction constant were also observed for Fe_{73.5}Cu₃Nb₄Si_{11.5}B₆ ribbon [11] and Fe_{73.5}Cu₁Nb₃Si_{13.5}B₇ and wire [12].

Magnetic hardening 112 was observed only for the Si-rich alloys after annealing at temperatures well below the 2nd stage of crystallization. This effect can be explained by the increase in the grain size of α -Fe(Si) phase. As already reported [13, 14, 15] the grain

diameter increases with the increasing annealing temperatures and decreasing boron concentrations in the amorphous alloys. This effect could also be related to the appearance of an additional crystalline phase which was identified to the copper. The precipitation of copper in Si-rich alloys can be justified because they have the highest volume fraction of α -Fe(Si) and therefore the highest relative concentration of copper in the intergranular layer. However, the significance of copper crystals as spinning centers for domain wall movements can be minimal if the crystals are very small.

The crystallization process and magnetic properties of $\text{Fe}_{73.5-x}\text{Co}_x\text{Si}_{13.5}\text{B}_9\text{Cu}_1\text{Nb}_3$ ($x=0, 5, 15, 29, 36, 45, 69, 73.5$) melt-spun alloys are analyzed as a function of x . For $x \leq 45$ ultrafine BCC α -FeSi(Co) crystallites (mean grain diameter in the range ~ 13 -16 nm) in an amorphous matrix are obtained after thermal treatments at 550°C (1h) while, for higher Co contents the precipitation of FCC β -Co rich crystallites is observed. For x up to 29, a slow increase in coercivity with x is observed that can be correlated, within the framework of the random anisotropy model, with the increase in the mean grain size of the α -FeSi(Co) crystallites with x . However for $x=36$ and 45, the nanocrystalline alloys manifest a noticeable magnetic softening compared with the alloys of lower Co content, which can be ascribed to a reduction in the magnetocrystalline anisotropy of the precipitated α -FeSi(Co) phase. Finally beyond $x=45$, the coercivity of the nanocrystalline alloys increases drastically, eventually by several orders of magnitude, reflecting the change to β -Co rich nanocrystallites.

For low-Co contents ($x \leq 29$), we propose that the magnetocrystalline anisotropy, K , of the precipitated α -FeSi(Co) phase remains almost constant, and that the main contribution to the increase in coercivity with x is the variation in mean crystalline diameter (H_c and d^6). A minimum value of K around $x=45$ would explain the decrease in coercivity observed in this composition region, while the sharp increase of H_c for $x \geq 69$ is ascribed to the magnetic decoupling of adjacent crystallites due to the sharp reduction of the exchange correlation length.

Nanocrystalline alloys can be obtained by a proper annealing treatment of metallic glasses, as reported in 1988 by Yoshizawa et al. [1]. The Fe-rich Fe-Cu-Nb-Si-B amorphous alloys crystallize in the form of ultrafine grains of α -FeSi embedded in

remaining amorphous matrix. The growth of the grains is controlled by the small fractions of Cu and Nb atoms. Excellent soft magnetic properties of these alloys (known under commercial name as FINEMET) are due to extremely low magnetic anisotropy and nearly zero saturation magnetostriction [16,17]. The reduction of the magnetostriction coefficient from 20×10^{-6} in amorphous state to about 1×10^{-6} in the nanocrystalline alloy results from competition between negative magnetostriction of the grains and the positive magnetostriction of the amorphous matrix [17,18]. Because of the small size of the grains of b.c.c-Fe-Si (an average diameter of nanocrystals is below 20 nm), it is believed that they are single domain particles. According to the theoretical model of Herzer [16], an exchange coupling between such nanocrystalline grains can effectively suppress the magneto-crystalline anisotropy of the individual grains. As a consequence of small effective anisotropy, the Fe-Cu-Nb-Si-B nanocrystalline alloys demonstrate huge permeability (of the order of 10^5) and low coercivity field (below 1 A m^{-1}). The question arises as to how the magnetic properties of the amorphous matrix affect the behavior of the nanocrystalline materials. The Fe-rich Fe-Cu-Nb-Si-B alloy seems to be a good object to study this problem. The microstructures of the alloys with Cr addition and of FINEMET show great similarities; however, the maximum available fractions of the nanocrystalline phase are much larger in FINEMET. Depending on the annealing conditions, these alloys are composed of α -Fe(Si) grains with diameters from 10 to 40 nm [19]. The content of Si in the grains was estimated from Mössbauer studies to be about 14 at.% [20]. It was also proved that Cr does not participate in precipitation of the b.c.c-Fe(Si) phase remaining in the amorphous matrix [20]. Increasing contents of Cr with the evolution of crystallization decreases the Curie temperature to $T_{\text{Cr}}=403 \text{ K}$) as well as the saturation magnetization of the amorphous matrix in comparison with values for the as-quenched amorphous alloy ($T_{\text{Cur}}=415 \text{ K}$). The curie point of the strongly ferromagnetic crystalline phase at about 920 K is well separated from that of the amorphous one. It is worth mentioning that superparamagnetic behavior of the grains was found in FeCrCuNbSiB alloys with 18% of the crystalline phase at temperatures above 523 K [21]. The aim of this work is to investigate the effect of the magnetization processes in Fe-rich nanocrystalline alloys on the basis of comparative studies of selected magnetic

properties of the $\text{Fe}_{73.5}\text{Cu}_1\text{Nb}_3\text{Si}_{13.5}\text{B}_7$ and $\text{Fe}_{66}\text{Cr}_8\text{Cu}_1\text{Nb}_3\text{Si}_{13}\text{B}_9$ nanocrystalline alloys at different stages of crystallization.

The annealing at 500°C is efficient in the formation of small crystalline fraction in FINEMET, whereas the alloy with Cr remains amorphous after such annealing. The maximum crystalline fraction in the FINEMET is over 2 times larger than in the alloys with Cr. The hysteresis loops of magnetization have been measured using a B-H loop tracer based on digital Fluxmeter Integrator EF4 (Magnet-Physik) and a data acquisition system. A coercive field and a maximum of the differential magnetic permeability (maximum slope of the B-H curves) have been evaluated from the hysteresis loops. The investigations of the reversible dynamic permeability have been carried out in the alternating magnetic field at a frequency of 10kHz and with a small amplitude of 5 A m^{-1} . A saw waveform of the biasing field with a frequency of 0.01 Hz has been used to magnetize samples. A study of the Barkhausen noise was limited to the measurements of the intensity (root mean square, rms) of the noise in the frequency band above 60 Hz. The peaks of the noise intensity have been determined for each sample. More advanced analysis of the noise was difficult because of weak Barkhausen effect in the samples with high crystalline fractions.

Interesting results have been obtained in the case of hysteresis loops of the $\text{Fe}_{66}\text{Cr}_8\text{Cu}_1\text{Nb}_3\text{Si}_{13}\text{B}_9$ nanocrystalline alloys. Representative curves of magnetization are in hysteresis loops have similar shapes for different fractions of the crystalline phase. The maximum slope of the curves changes only slightly with the evolution of crystallization in comparison with a dramatic increase of the coercivity. It is worth mentioning that similar shapes of the hysteresis loops have been predicted by the Stoner-Wohlfarth model for magnetization rotations in single domain particles with anisotropy axis inclined by about 10° to the direction of the external magnetic field.

It is important to notice that the dynamic reversible permeability demonstrates quite different dependence on the crystalline fraction than the differential permeability determined from the hysteresis loops. This feature can be easily understood in the case of a rotational mechanism of magnetization: namely, the differential permeability is related to the reversible rotations of the magnetization, leading to high slopes of hysteresis loops

(as in the Stoner-Wohlfarth model). On the other hand, the reversible permeability refers to small reversible deviations of magnetization of vectors forced by weak alternating magnetic field and it is closely related to the magnetic anisotropy as well as coercivity. The Barkhausen effect turns out to be very helpful in the interpretation of the magnetization process in the nanocrystalline materials. The Barkhausen effect [22] is a result of discontinuous changes of magnetization as a response to a smoothly changing external magnetic field. These sudden jumps of magnetization in soft magnetic arise from interactions of the domain walls with imperfections of the material, such as grain boundaries, residual stresses, or magnetic and non-magnetic precipitations. Modern theoretical models, e.g. Ref. [23], assume that the Barkhausen noise depends among other things on the saturation magnetization, magnetization rate and permeability of a magnetic material. Large Barkhausen jumps are expected in the materials with high saturation magnetization, huge permeability and large coercive field, which represents strong pinning forces. This is just the case of the $\text{Fe}_{66}\text{Cr}_8\text{Cu}_1\text{Nb}_3\text{Si}_{13}\text{B}_9$ nanocrystalline alloys, on the contrary, a small Barkhausen effect should result from either small magnetization and permeability or from weak coercivity, which is characteristic of homogenous materials without pinning centers, as in the case of FINEMET. The nanocrystalline grains in the Fe-Cu-Nb-Si-B alloy are considered to be too small (i.e., several times smaller than the domain wall width) to act as pinning centers for domain wall movements. Because of the lack of other inhomogeneities in these materials, they exhibit small magnetic hysteresis and also weak Barkhausen noise which is more than one order of magnitude smaller than in the as-quenched $\text{Fe}_{73.5}\text{Cu}_1\text{Nb}_3\text{Si}_{15.5}\text{B}_7$ amorphous alloys.

In spite of similarities in the microstructure of the $\text{Fe}_{73.5}\text{Cu}_1\text{Nb}_3\text{Si}_{15.5}\text{B}_7$ and $\text{Fe}_{66}\text{Cr}_8\text{Cu}_1\text{Nb}_3\text{Si}_{13}\text{B}_9$ nanocrystalline alloys, their magnetic properties differ considerably from each other. The alloys of the FINEMET composition exhibit a tendency to magnetic softening with increasing fraction of the nanocrystalline phase, whereas the alloys with Cr addition become magnetically harder. The behavior of these 2 alloys is a result of the different saturation magnetization of the amorphous matrixes and, consequently, different magnetic coupling suppresses magnetic anisotropy of individual grains in the Fe-Cr-Cu-Nb-Si-B alloy, contributing to the improvement of soft magnetic properties. Magnetic hardening of the Fe-Cr-Cu-Nb-Si-B alloy with the evolution of the

crystallization process is associated with the anisotropic properties of the crystalline grains.

Yoshizawa et al [24] and Noh et al [25] studied the effect of Cu on the crystallization behavior in *F74.5Cu0Nb3Si13.5B9*. They found that, the average grain size at the onset of crystallization is relatively large due to lower nucleation rate with no addition of Cu and annealing of this Cu free alloy leads to the simultaneous or sequential formation of several crystalline phases. The effect of Cu, in enhancing the nucleation density is unique.

Substituting Nb by other group V or VI refractory elements (Cr, V, Mo, W or Ta) in FINEMET, Yoshizawa et al. [26] and Muller et al [27] showed that like Nb, the atomic volumes of these refractory elements are larger than that of Fe. This reduces the diffusion coefficients and, thus, stabilizes the amorphous matrix and slows down the kinetics of grain coarsening.

Alben, et al. [28], Sawa et al. [29] and Suzuki et al. [30] reported on the relation of grain size and the domain wall width. If the grain size exceeds the domain wall width, domains can be formed within the grains and the coercive field, H_c is found to depend on the grain size, D as $H_c \propto D^{-1}$.

1.5 Aim of this Work

A nanocrystalline Fe-Si-B-Nb-Cu alloy, known as FINEMET, is a very attractive soft magnetic material exhibiting excellent permeability while maintaining a high saturation magnetization [1]. [1] Y. Yoshizawa, S. Oguma, and K. Yamauchi, *J. Appl. Phys.* 64 (1988), p. 6040.

These materials are interesting from both the fundamental and applied viewpoints. Because of various superior mechanical, magnetic and electrical properties, in comparison with those of the crystalline state, FINEMET-type nanocrystalline alloys

(metallic glasses) form a class of technologically important materials. They have already been put into applications in the devices e.g., choke coils, high frequency transformers and the magnetic thin film heads.

The objective of this research is to study the effect on electrical resistivity, magnetoresistance, hall-coefficient, impedance, frequency dependent complex magnetic permeability. The studies involved in the present work would provide useful information about its potential applications in high frequency switching devices. In order to achieve the aforesaid objective, the following main steps are included in the present work:

1. Measurements of magneto-resistive properties in different magnetic fields
2. The zero field cool (ZFC) and field cool (FC) measurements to observe the aging effect (Spin-Glass)
3. The measurement of permeability in the high frequency range (frequency range: 1MHz ~1.5 GHz) for annealed Fe73-Cu1-Nb3.5-Si-14B-8.5 magnetic alloy at room temperature.
4. The measurement of Magnetization at room temperature by VSM(Vibrating sample magnetometer)

Chapter-2: Theoretical Aspects

2.1 Formation of Nanocrystalline state

Nanocrystalline soft magnetic materials (Metallic glasses) have been found to be promising for technological applications since its discovery by Yoshizawa et al [1] in 1988. The first class of such materials was the melt-spun *Fe-Si-B* alloys containing small amounts of *Cu* and *Nb*. The *Fe-Si-B-Nb-Cu* amorphous phase transforms to a body centered (bcc) *Fe-Si* solid solution with the grain sizes of about 10 nm during annealing above the crystallization temperature. The resulting microstructure is characterized by randomly oriented, ultra fine grains of bcc Fe-Si (20 at %) with typical grain size of 10-50 nm embedded in a residual amorphous matrix which occupies about 20-30% of the volume and separates the crystallites at a distance of about 1-2 nm.

However, to achieve the nanocrystalline state, amorphous ribbons are obtained by a quenching procedure followed by heat treatment at 500 - 600 Nanocrystalline materials are polycrystalline solids with very small crystallites (diameters about 5 - 20nm). These materials contain a large number of interfaces with random orientations and a substantial fraction of atoms located in these interfaces.

The presence of *Cu* helps to increase the nucleation rate of the bcc phase while *Nb* retards the grain growth. These nanocrystalline materials have emerged as FINEMET alloys. They provide low core losses (even lower than amorphous soft magnetic alloys such as *Co-Fe-Si-B* system), exhibit saturation induction of about 1.2 Tesla and very good properties at high frequencies comparable to the best *Co based* amorphous alloys. Many of the soft magnetic properties of FINEMET-type nanocrystalline alloys are found superior. They exhibit lower saturation induction than *Fe-* metalloidal amorphous alloys mainly because of the lower *Fe* content to attain amorphization and the addition of *Cu* and *Nb* (or other elements to control the nucleation and growth kinetics). The small single-domain nanocrystalline *Fe* particle in the amorphous matrix gives these

alloys their unique magnetic behaviour; the most dramatic one is the lowest energy losses (narrowest B/H hysteresis loop) of any known materials along with very high permeability and nearly or exactly zero magnetostriction.

2.2 Microstructure and effects of grain size

It was commonly known that the characteristics of soft magnetic materials are “larger crystal grains yield better soft magnetic properties”. Contrary to this common belief, soft magnetic material consisting of a small, “nano-order”, crystal grains have excellent soft magnetic properties.

Figure 1 shows a typical electron micrograph of Fe-13.5Si-9B-3Nb-1Cu alloy produced by the primary crystallization process from the melt-spun amorphous ribbon. This consists of the nanocrystalline bcc phase with an average grain size of approximately 10 nm. There is no preferred orientations in the grains. In addition to grains of ~10 nm, smaller grains can be recognized as indicated by arrowheads. These are now known to be fcc Cu particles which precipitated out in the early stage of crystallization. For producing such nanocrystalline microstructure, it is reported that a combined addition of Nb and Cu is required [2], thus the role of Nb and Cu for nanocrystallization was of great research interest. Atom probe field ion microscopy was found to be an extremely effective technique to study solute clustering, precipitation, segregation and partitioning behaviors, in fact great contribution to the understanding of nanocrystallization mechanism were made by a conventional atom probe [31-34].



Fig.2.1 A typical TEM bright field image of $\text{Fe}_{73.5}\text{Si}_{13.5}\text{B}_9\text{Nb}_3\text{Cu}_1$ rapidly solidified alloy. The nanocrystalline bcc phase with an average grain size of ~10nm.

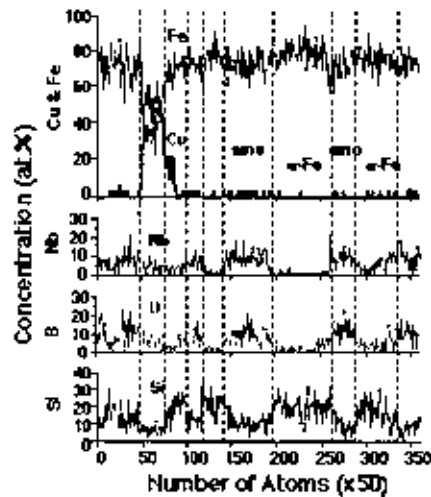


Fig. 2.2 Concentration depth profile of $\text{Fe}_{73.5}\text{Si}_{13.5}\text{B}_9\text{Nb}_3\text{Cu}_1$ alloy annealed at 550°C for 60min. The presence of three types of phases are clearly identified.

Figure 2.2 shows atom probe concentration depth profiles of the $\text{Fe}_{73.5}\text{Si}_{13.5}\text{B}_9\text{Nb}_3\text{Cu}_1$ alloy with the optimum magnetic properties (annealed at 550°C for 60 min.). The presence of three types of phases are clearly identified. One is enriched with Si (~20-25 at.%) but contains little Nb, Cu and B. Complementary TEM observations suggested that this region was the crystallized bcc α -Fe phase containing Si. In addition to the α -Fe grains, a B and Nb enriched amorphous phase is present with little Cu content but containing certain amount of Si. In addition to these two phases, a Cu enriched particle is observed. This phase was significantly enriched in Cu (~60%) but still contains appreciable amounts of the other elements. Since the concentration of Fe is only about 30%, this phase is believed to be nonmagnetic. In fact, a separate nanobeam electron diffraction study in a transmission electron microscope (TEM) revealed that the Cu enriched particles were fcc Cu. This phase appears as a grain having a diameter of approximately 5 nm as indicated by arrows in Fig. 2.1.

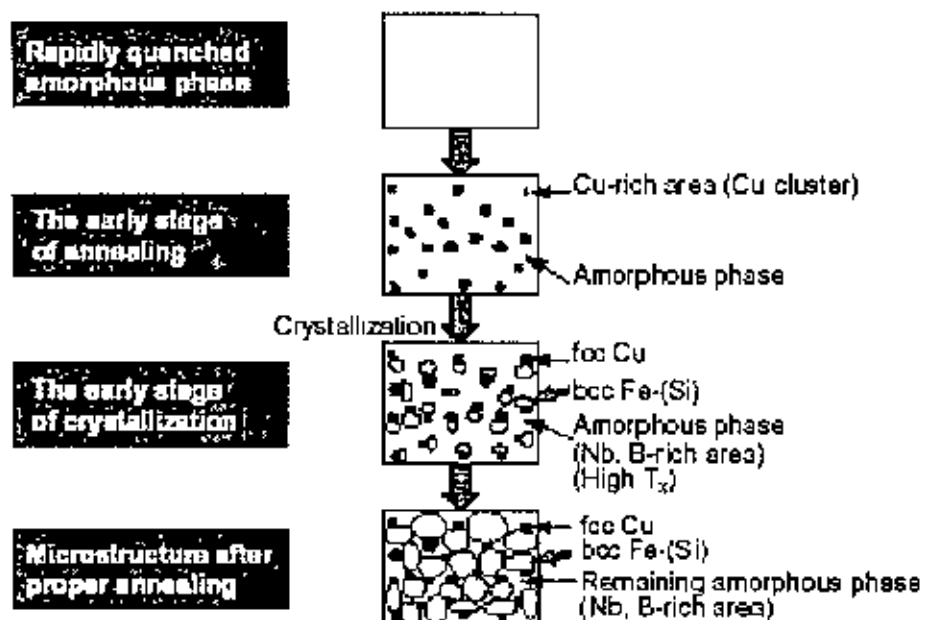


Fig.2.3 Crystallization process of FINEMET

Fig. 2.3 shows the crystallization process. At the final stage of this crystallization process, the grain growth is suppressed by the stabilized remaining amorphous phase at the grain boundaries. This stabilization occurs because the crystallization temperature of the remaining amorphous phase rises and it becomes more stable through the enrichment of Nb and B. Synergistic effects of Cu addition, "which causes the nucleation of bcc-Fe" and Nb addition, "which suppresses the grain growth" creates a uniform and very fine nanocrystalline microstructure.

Fig. 2.4 shows the relationship between crystal grain diameter (D) and coercive force (H_c) for soft magnetic materials. In the conventional soft magnetic materials, "whose grain size is far larger than $1\mu\text{m}$ ", it was well known that soft magnetic properties become worse and coercive force increases when crystal grain size becomes smaller. For example, coercive force is thought to be inversely proportional to D . Therefore, main efforts to improve the soft magnetic properties were directed to make the crystal grain size larger and/or to make the magnetic domain size smaller by annealing and working. However, FINEMET demonstrated a new phenomenon; reduction of grain size, "to a nano-meter level", improves the soft magnetic properties drastically. In this nano-world, the coercive force is directly proportional to D on the order of D^2 to D^6 . This is absolutely contrary to the conventional concepts for improving the soft magnetic properties.

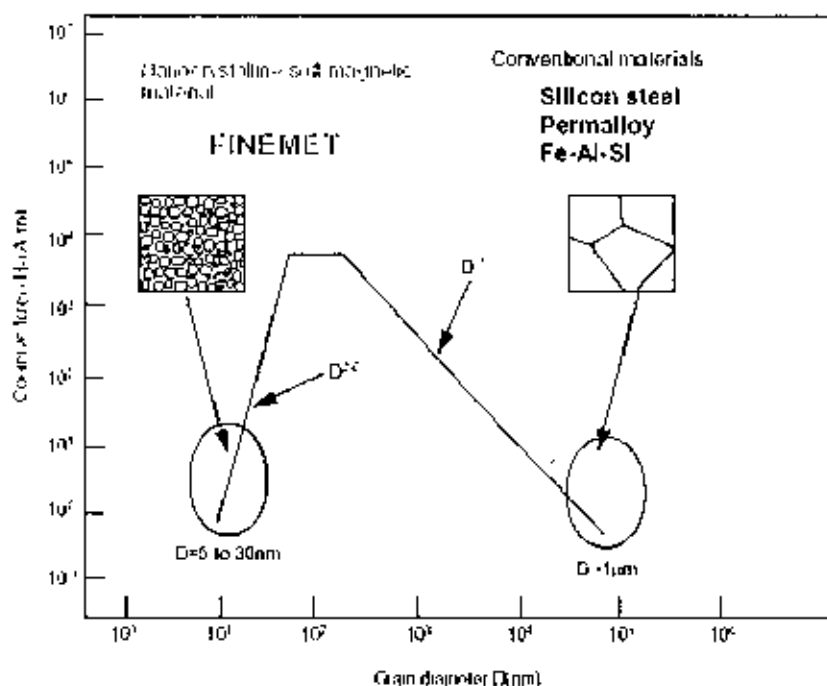


Fig 2.4 Relationship between crystal grain diameter (D) and coercive force (H_c)

2.3 Temperature Dependence of the Magnetic Properties

The Exchange interaction between the bcc grains mainly occurs via the interfacial amorphous minority matrix in which the nanocrystalline are embedded. When measuring temperature approaches the Curie temperature, T_c of the intergranular amorphous phase, which is much lower than T_c of the bcc grains, the exchange coupling between the crystallites is largely reduced. As a result, the initial permeability, μ_i then drops down during the initiation of crystallization [35] and the coercivity, H_c increases correspondingly. Simultaneously, the domain structure changes from wide domains to a pattern of small, irregular domains. With increasing measuring temperature the coercivity reaches a maximum and, finally decreases towards zero at temperature below the Curie temperature of the bcc grains. This indicates the transition to superparamagnetic behavior [36]. The exchange of the coupling decrease with increasing temperature due to the simultaneous decrease of the magnetization in the bcc grains. Consequently, the soft

magnetic properties keep on degrading even above T_c^{am} until thermal energy dominates and the system gets superparamagnetic. It is very important to inhibit the formation of Fe-B compounds to guarantee the magnetic softness of the ultrafine bcc grain structure. Thus, annealing above certain temperature leads to the precipitation of the Fe-B with typical dimension, while the ultrafine grain structure of bcc Fe-Si still persists.

The temperature dependence of the magnetic properties demonstrates that it is important to maintain an efficient exchange coupling between grains by appropriate alloy design such that the Curie temperature of the residual amorphous matrix is clearly higher than application temperatures.

2.4 High Frequency Behavior and Losses

The frequency dependence of permeability and the core losses of the nanocrystalline Fe-Cu-Nb-Si-B alloys behave advantageously compared to those of other amorphous alloys. The use of nanocrystalline soft magnetic alloys at higher frequencies will be favorable for small electronic device. The magnetic properties of initial permeability (μ_i) may be strongly affected by the presence of an electric current, particularly in ac condition. The measurement of magnetic properties as a function of frequency and its analysis by means of the complex permeability formalism has recently led to the resolution of several aspects of the magnetization process [36,37,38]. The measurement of complex permeability gives valuable information about the nature of the domain wall and their movements.

2.5 Magnetization of Nanocrystalline Alloys

Magnetization is defined as the magnetic moment per unit volume or mass of the specimen. A ferromagnet has a spontaneous magnetic moment even in zero magnetic fields. A spontaneous moment suggests that electron spins and magnetic moments are arranged in a regular manner. Below the Curie temperature, the electronic magnetic moments of a ferromagnet are essentially all lined up. The magnetic moment may be very much less than the saturation moment, and the application of an external magnetic field

may be required to saturate the specimen. Actual specimens are composed of small regions called domains, within each of which the local magnetization is saturated. Domains grow or contract in volume due to domain boundary movements when the material is acted upon by a changing magnetic field. The directions of magnetization of different domains need to be parallel. The increase in the magnetic moment of the specimen under the action of an applied magnetic field takes place by two independent processes:

1. In weak applied fields the volume of domains favorably oriented with respect to the field increases at the expense of unfavorably oriented domains.
2. In strong applied fields the magnetization rotates toward the direction of the field.

From the Hysteresis loop, the coercive force is defined as the reverse field needed to reduce the induction B or magnetization M to zero, starting in a saturated condition. The remanence B_r is the value of B at $H=0$. The saturation induction B_s is defined as the limiting value of $(B-H)$ for large H . The saturation magnetization M_s the most sensitive property of ferromagnetic materials, which is subject to control. The domain structure of ferromagnetic materials affects their practical properties such as coercivity, permeability etc.

Amorphous alloys are basically metastable materials. When they are annealed well below the crystallization temperature, structural relaxation can occur. It increases M_s which leads almost line Hysteresis curve. The decrease of M_s above the crystallization temperature corresponds to the optimum nanocrystallised state with high volume fraction of Fe (Si) nanograins [39].

2.6 Electrical Resistivity

Resistivity, ρ is actually the characteristic property of metals, given as A

$$\rho = R \times \frac{A}{l} \text{ ohm-meter (2.2)}$$

where, l is the length and A is the cross-sectional area of the material. The conduction electrons are responsible for the current flow. The electron undergoes a collision only because the lattice is not perfectly regular. We group the derivations from a perfect lattice into two classes:

- a. Lattice vibrations (phonons) of the ions around their equilibrium position due to thermal excitation of the ions.
- b. All static imperfections, such as foreign impurities or crystal defects.

Now we can write,

$$\rho = \rho_{ph} + \rho_i \quad (2.3)$$

It is seen that ρ has split into two terms: a term ρ_i is due to scattering by impurities, which is independent of T , called residual resistivity. Another term added to this is ρ_{ph} arises from the scattering by phonons and therefore temperature dependent. This is called ideal resistivity.

At low temperature T , scattering by phonons is negligible because the amplitudes of oscillations are very small; in that region $\rho_{ph} \rightarrow 0$ and hence $\rho = \rho_i$, is a constant. As T increases, scattering by phonons becomes more effective and $\rho_{ph}(T)$ increases; this is why ρ increases. When T becomes sufficiently large, scattering by phonons dominates and $\rho \cong \rho_{ph}(T)$. In the high-temperature region, $\rho_{ph}(T)$ increases linearly with T . Resistivity linearly increase with T up to the melting point for the case of pure element. On the other hand, the electrical resistivity of metallic glass is measured to be very high due to the disorder arrangement of the atoms. The electrons suffer enormous scattering as they pass

through the disorder matrix of ions. Thus the mean free paths of the conduction electrons are very short and hence the drift velocities of the electrons are very low giving the material a property of high electrical resistivity. This resistivity may drop quite abruptly at a certain temperature as the temperature of the sample is increased. The increase in temperature gives rise to the formation of small regions of ordered phases at the onset of segregation and thus attaining the crystalline phase when the resistivity falls sharply at the crystallization temperature. This unique property of the metallic glass is of very interesting to the people who are working with the commercial applications of metallic glasses e.g., the power supplies, transformers, magnetic heads, magnetic shielding etc.

2.7 Magnetoresistance of the Amorphous Alloys

The phenomenology of the magnetoresistance effect is similar to that of magnetostriction. This effect can be classified into two categories: one depends on the intensity of spontaneous magnetization that corresponds to the volume magnetostriction [40]. The second is caused by the rotation of spontaneous magnetization corresponds to the usual magnetostriction. N.F.Mott [41] interpreted this phenomenon in terms of the scattering probability of the conducting electrons into $3d$ holes. If the substance is in a ferromagnetic state, half of the $3d$ shell is filled up, so that the scattering of $4s$ electrons into the plus state of $3d$ shell is forbidden. This scattering is however, permitted in a non magnetic state in which both the plus spin state and the minus spin state of the upper $3d$ levels are vacant. Mott explained the temperature variation of resistivity fairly well by this model. T.Kasuya [42] interpreted this phenomenon from a standpoint quite different from Mott theory. He considered that d electrons are localized at the lattice points and interact with conduction electrons through the exchange interaction. At 0 K the potential for the conduction electrons is periodic, because the spins of $3d$ electrons of all the lattice points point in the same direction. At finite temperature, spins of $3d$ electrons are thermally agitated and the thermal motion may break the periodicity of the potential. The $4s$ electrons are scattered by an irregularity of the periodic potential which results in additional resistivity. T. Kasuya postulated that the temperature dependence of the resistivity of ferromagnetic metals is composed of a monotonically increasing part due to

lattice vibration and an anomalous part due to magnetic scattering, the magnitude of the later being explained by this theory. The magneto-resistance, therefore, refers to the change in electrical resistance of a crystal in response to the magnetic field applied to the specimen externally. This effect is due to the fact that when the magnetic field is imposed, the paths of the electrons become curved and do not go exactly in the direction of the superimposed electric field.

2.8 Spin -Glass behavior of Amorphous alloy

A spin glass is a magnetic material in which the exchange interaction, J_{ij} , between atomic spins S_i , is a random variable. as usual, a positive sign of the exchange interaction favors parallel alignments of a spin pair, while a negative sign favors an antiparallel alignment. A consequence of such random exchange interactions between the moments is a frustrated system i.e. for a representative spin there is no obvious direction relative to its neighbors to align. The free energy minimization of the system becomes a non-trivial optimization problem.

To describe a spin glass Edwards and Anderson [44] proposed the following Hamiltonian

$$H = \sum_{\langle ij \rangle} J_{ij} S_i S_j + H \sum_i S_i$$

Where H , is an applied magnetic field. In the Ising model an “up” spin takes the value $S=1$ and accordingly $S=-1$ for a “down” spin. Usually the interactions are picked randomly from a symmetrical distribution fulfilling $[J_{ij}] = 0$ and $[J_{ij}^2] = J^2$ ([...] denotes an average value), but also a non-zero value is motivated in some cases.

From experimental, numerical and theoretical studies, it is now generally believed that the lower critical dimension for a short range Ising Spin- glass is between 2 and 3 [46, 47,48,49] i.e. a finite spin glass phase transition temperature T_g , exists in 3 dimensions but not in 2 dimensions. For the isotropic vector spin-glasses the situation is less clear. While some theoretical and numerical work predicts the absence of a spin- glass phase [50(10)], other work [51.52(11,12)] gives arguments in favor of the existence of a low

for RKKY- interacting spin-glasses is three and the universality class is expected to be different from short range interacting spin-glasses.

Random interactions between moments can be observed in materials where the Rudderman-Kittel_Kasuya-Yosida (RKKY) interaction [54] is dominant, i.e. where the magnetic moments are coupled via the induced polarization in the electron gas of the host material. examples of the such metallic spin-glasses are the alloys Cu(Mn), Ag(Mn) and Au(Fe). in the three dimensional free electron approximation, the RKKY interaction can be written as [54]

$$J_{\text{RKKY}} \propto \frac{\cos(2K_f r)}{(K_f r)^3}$$

where k_f is the magnitude of the wave vector at the Fermi surface. With increasing distance r , between spin pairs, the interaction falls off as r^{-3} and oscillates in sign.

Another way of achieving random exchange coupling is by mixing compounds such as the insulating ilmenites FeTiO_3 and MnTiO_3 [55,56]. In this case the crystal structure can be described as a layered honeycomb structure where the magnetic ions Fe^{2+} or Mn^{2+} , are situated in planes separated by a layers of Ti^{4+} ions. Within the planes, Fe^{2+} ions coupled ferromagnetically but antiferromagnetically between the planes. For Mn^{2+} ions, both the inter- plane and intra- plane interactions are antiferromagnetic. By mixing Fe and Mn the crystal growth process, each magnetic site becomes randomly occupied by either a Fe^{2+} or Mn^{2+} ion. Consequently Frustrations appears and a spin- glass ordered phase is formed at low temperatures for a three dimensional system. By denoting the mixed compound as $\text{Fe}_x\text{Mn}_{1-x}\text{TiO}_3$ a spin- glass phase is formed for x in the range $0.38 < x < 0.58$. For other values of x the system displays an antiferromagnetic phase which additionally, for x close to the limits of the range giving a pure paramagnetic- spin -glass transition, re-enters into a spin-glass phase as the temperature decreased. Systems with this property are called re-entrant spin-glasses.

The main difference between the metallic spin glasses and $\text{Fe}_x\text{Mn}_{1-x}\text{TiO}_3$ is that while the RKKY interaction is long ranged in the former systems, the exchange interaction only extends over a few lattice sites in the latter. Furthermore, due to the elongated electron orbitals of the Fe^{2+} ions and the dipole dipole interaction between the Mn^{2+} ions, the latter system is highly anisotropic and therefore becomes good model system for Ising spin-glass.

Chapter-3: Method of Sample Preparation

3.1 Method of Sample Preparation

The alloy composition $Fe_{73.5}Cu_1Nb_{3.5}Si_{14}B_{18.5}$ can be considered as atypical Fe-Si-B metallic glass composition with small addition of Nb. The alloy system has a good glass forming ability. Controlled crystallization from the amorphous state is the only method presently available to synthesize nanocrystalline alloys with attractive soft magnetic properties. To understand the properties possessed by nanocrystalline materials, identification and development of suitable preparation methods need serious attention. Applying various methods where the atomic arrangements have no long-range periodicity can produce metallic alloys in an amorphous state. The different methods are generally classified into two groups:

- [1] The fast cooling of the melt.
- [2] The atomic deposition methods

3.1.1 The Fast Cooling of the Melt

By using any of the liquid quenching device an amorphous state can be produced where the alloys must be cooled through the temperature range from the melting temperature (T_m) to the glass transition temperature (T_g) very fast allowing no time for crystallization. The factors controlling T_g and crystallization are both structural and kinetic. Atomic arrangement, bonding and atomic size effect are related in the structural factors. Turnbull [51] discussed the kinetic factors in which the nucleation, crystal growth rate and diffusion rate are compared to the cooling rate. The methods using the principle of fast cooling of melt techniques are:

- [1] The gun techniques
- [2] Single roller rapid quenching techniques
- [3] Double roller rapid quenching techniques
- [4] Centrifuge and rotary splat quencher techniques
- [5] Torsion catapult techniques
- [6] Plasma-jet spray techniques
- [7] Filamentary casting techniques
- [8] Melt extraction techniques
- [9] Free-jet spinning techniques
- [10] The melt spinning techniques.

Although the various techniques used in preparation amorphous ribbons, only the single roller rapid quenching technique, which used to prepare the ribbons for the present work is discussed below:

3.1.2 Rapid Quenching Method

Duwez and his collaborators [43] first discovered this method in 1960. The apparatus of rapid quenching technique is shown in the fig. 3. 1. It consists oh mainly a copper roller, an induction heater and a nozzle. A variable speed motor is driven the roller via a tooth belt. The material of copper roller was chosen for its good conductivity and mechanical softness that allowed cleaning and polishing to be carried out easily. Quartz tube is suitable for repeated use in several successful runs and should be transparent to make the melting process visible. It should withstand the sudden fast changes in temperature.

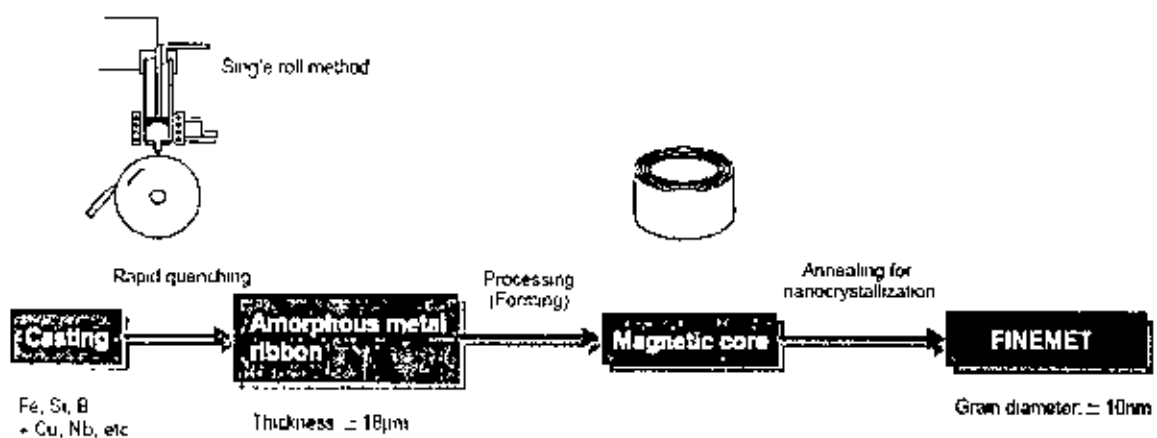


Fig.3.1 Manufacturing process of "FINEMET"

3.2 Important Factors to Control the Thickness of Ribbons

[1] Rotating speed

Angular velocity $w = 2000$ revs./min. and

Surface velocity $v = 25$ m/s

[2] Gap between nozzle and rotating copper drum $h = 100$ to 150 μ m

[3] Oscillation of the rotating copper drum both static and dynamic has maximum displacement 1.5 to 5 μ m.

[4] Pressure = 0.2 to 0.3 argon atmosphere

[5] Temperature of metals T , 1500°C . The temperature did not exceed 1800°C otherwise quartz tube would be melt.

[6] Stability was ensured for the drop in the surface of drum.

3.3 Conditions for the Formation of Nanocrystalline Materials

A basic condition For the Formation of a typical nanocrystalline material is given by-

- [1] The magnetic properties are highly dependent on grain size; if the grain size were longer, the magnetic anisotropy would be very high; which in turn will have diverse effect on the soft magnetic properties specially the permeability.
- [2] There should be nucleation centers initiated for the crystallization process to be distributed throughout the bulk of amorphous matrix.

- [3] There must be a nucleation for stabilizing the crystallites.
- [4] Nanocrystalline materials obtained from crystallization must be controlled so that the crystallites do not grow too big. The grain growth should be controlled so that the grain diameter is within 15 - 20 nm.
- [5] The size of the grains can be limited to nanometer scale by doping group -11 metals etc. Cu(Ag.....)
- Nb, W, Mo, Cr, Ta etc.
- [6] The stability must be lower and the crystallization temperature must be higher.

Experimental Details

3.4 Resistivity Measurement

According to the Ohm's law for electrical conduction in metals,.

$$I = \frac{V}{R} \quad (3.4.1)$$

where, I is the current, V is the potential difference, and R is the resistance. From laws of resistance, we know that

$$R = \rho \frac{L}{A}$$

Here ρ is the proportionality constant called resistivity as:

$$\rho = R \times \frac{A}{l} \quad \Omega \text{ — meter} \quad (3.4.2)$$

where, R is the resistance of the sample, A is the cross-sectional area, which is the product of the width and thickness. However, to measure the resistance at different magnetic fields ($H = 0 - 4$ kOe) function of temperature, modified 4-probe method has been used figure 3.2 with the following experimental setup. Therefore using equation (3.4.2) we calculate the required temperature dependence of resistivity.

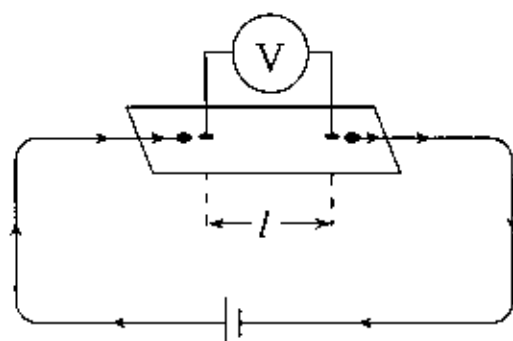


Fig.3.2 Four-point probe technique to measure resistivity

3.5 I-V Measurement at Room Temperature

The sample is placed between two pole pieces of electromagnet. Field current calibrates the magnetic field. Then for various magnetic fields, calibrated field current is supplied to the field coil of the electromagnet. Keeping the current constant at that value, for various currents (10 to 200 mA with an interval of 10 mA) passed through the sample from the regulated power supply in constant current mode; corresponding voltage across the inner two probes has been recorded by the digital voltmeter.

3.6 I-V Measurement at high Temperature

Figure-3.3 shows the schematic diagram of the experimental setup for I-V measurement at high temperature (300 to 720K). This is almost same as the room temperature measurement procedure. The difference is that the sample in this case is kept inside the evacuated high temperature oven. In addition to the setup as discussed above, the temperature is calibrated against the microvolt. In this measurement, it is very important that the high temperature oven must not interact with the sample. So, the most important feature in the construction of the high temperature oven is that the inner stainless tube extends throughout the oven and the thermocouple unit is inserted from the bottom end with the thermocouple junction placed immediately below the sample.

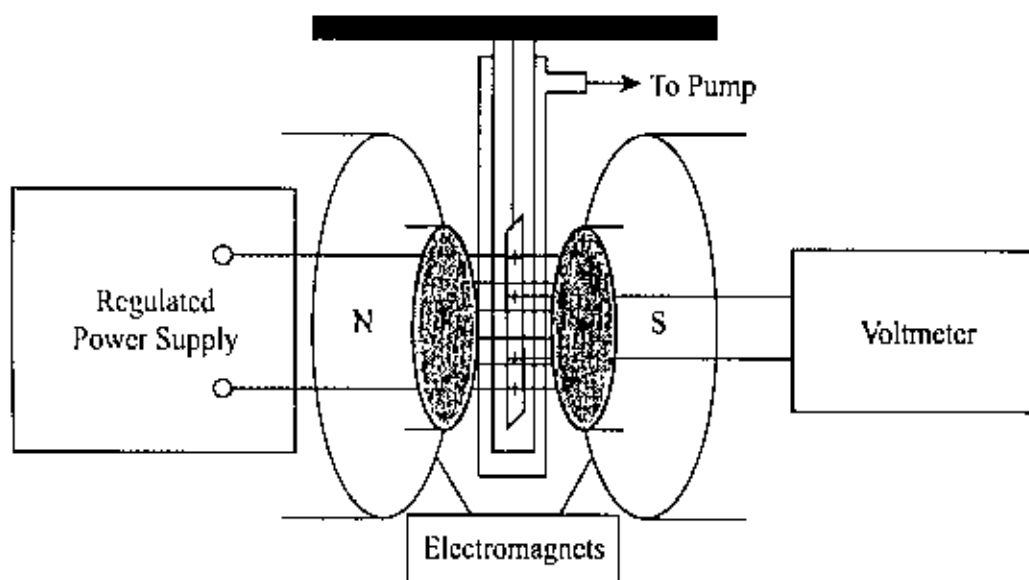


Figure-3.3 The schematic diagram of the experimental setup for I-V measurement at high temperature

The heater is wound directly on the inner tube. The heater consists of MgO insulated Chromel-Constantan couple with a stainless steel cover (O.D 1mm, length 1.3 m, manufactured by OMEGA Corp) This thermocouple is flexible, and to obtain a firm contact between the heater and the inner sample tube, the thermocouple is first wound on a tube with a somewhat smaller diameter and the resulting spiral is afterwards squeezed on to the sample tube. The thermal contact between the heater and the sample tube is improved by adding some silver paint. The lower ends of the heater wires are electrically connected by means of silver paint. Copper wires, connecting an external power supply, are soft soldered on the upper ends of the heater wires. The silver paint is dried out at ordinary atmosphere by passing some current through the heater. The advantages to use this Chromel-Constantan thermocouple as a heater for this oven are that it is readily available, non-magnetic, insulated, easily formed and gives a bifilar winding and close thermal contact with the sample tube. The heater has a resistance of 75 ohms at room temperature. Five radiation shields, consisting of 50-micron stainless steel foils are located outside the heater. These are tied on to the heater using reinforced glass fiber threads. The outer tube is at the bottom end connected to the inner tube via a phosphor bronze below in order to allow for the difference in length of the

two tubes at higher temperatures. O-ring couplings are used through to enable easy disassembling of the oven in case of any fault. Both the oven and the thermocouple are adjustable in height with respect to sample. This gives the possibility to find a position of the sample in the warmest region of the oven, which gives a minimum temperature gradient between the sample and the thermocouple junction.

The temperature gradient $\frac{\Delta T}{T - T_0}$ over 10 mm of length in the warmest part of the oven

is approximately 0.1% and independent of the temperature.

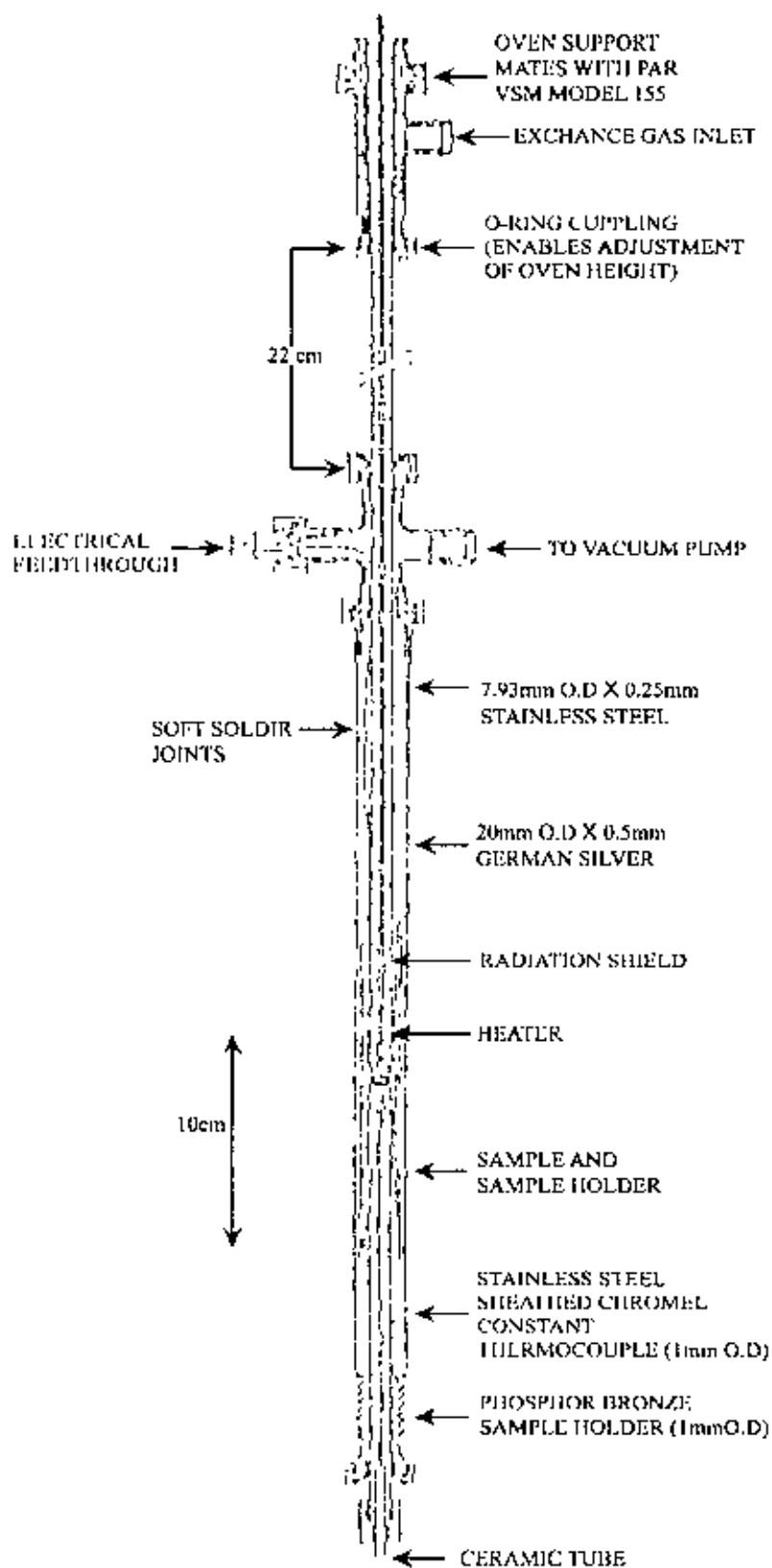


Figure-3.4 Schematic diagram of such a high temperature oven.

3.7 Magnetoresistance Measurement

Magnetoresistance is measured from the calculation of magnetic field dependent resistance, which discussed in section 3.9. By the definition of magnetoresistance, it is given by

$$MR\% = \frac{R_H - R_0}{R_0} \times 100 \quad (3.7.1)$$

Where, R_0 is the resistance at magnetic field $H = 0$ kG and R_H is the resistance at magnetic field, $H = 1$ kG, 2 kG, 3 kG, 4 kG.

3.8 Measurement of Magnetisation

Magnetisation is defined as the magnetic moment per unit volume or mass of the specimen. There are various ways of measuring Magnetization of a substance. In the present thesis Magnetization has been determined by using Vibrating Sample Magnetometer (VSM) at room temperature applying the magnetic field from 0 kilogauss to 6.2 kilogauss.

3.9 Working Principle of Vibrating Sample Magnetometer (VSM)

The vibrating sample magnetometer has become a widely used instrument for determining magnetic properties of a large variety of materials: diamagnetic, paramagnetic, ferromagnetic, ferromagnetic and antiferromagnetics. It has a flexible design and combines high sensitivity with easy of sample mounting and exchange. Samples may be interchange rapidly even at any operating temperature. Measurements of magnetic moments as small as 10^{-3} emu are possible in magnetic fields from 0 to 6.2 Tesla.

3.9.1 Principle

If a sample of any material is placed in a uniform magnetic field, created between the poles of an electromagnet, a dipole moment will be induced. If the sample vibrates with sinusoidal motion a sinusoidal electrical signal can be induced in suitably placed pick-up coils. The signal has the same frequency of vibration and its amplitude will be proportional to the magnetic moment, amplitude, and relative position with respect to the pick-up coils system. Pickup coils work by Faraday's law of induction.

$$\varepsilon = d\phi/dt \quad (3.9.1)$$

where, ε is the voltage induced, ϕ is the change in magnetic flux in time t . As the M field is static there is no ϕ , so a pickup coil cannot work. To overcome this problem the sample is vibrated using a sinusoidal oscillation. This vibration generates the required change in flux with respect to time and produces a signal from the pickup coils.

The sample is fixed to a small sample holder located at the end of a sample rod mounted in an electromechanical transducer. The transducer is driven by a power amplifier which itself is driven by an oscillator at a frequency of 90 Hertz. So, the sample vibrates along the Z axis perpendicular to the magnetizing field. The latter induced a signal in the pick-up coil system that is fed to a differential amplifier. The output of the differential amplifier is subsequently fed into a tuned amplifier and an internal lock-in amplifier that receives a reference signal supplied by the oscillator. The output of this lock-in amplifier, or the output of the magnetometer itself, is a DC signal proportional to the magnetic moment of the sample being studied. The electromechanical transducer can move along X , Y and Z directions in order to find the saddle point (which Calibration of the vibrating sample magnetometer is done by measuring the signal of a pure Ni standard of known the saturation magnetic moment placed in the saddle point.

3.10 Permeability Measurement

For high frequency application, the desirable property of a soft magnetic material is the high permeability with low loss. The present goal of the research is to fulfill this requirement. Theory and mechanisms involved in permeability are discussed below.

3.10.1 Theory of Permeability

Permeability is defined as the proportionality constant between the magnetic field induction B and applied intensity H ;

$$B = \mu H \quad (3.10.1)$$

This definition needs modification when magnetic material is subjected to an ac magnetic field as given below

$$H = H_0 e^{j\omega t} \quad (3.10.2)$$

In such a field the magnetic flux density experiences a delay with respect to H . The delay is caused due to the presence of various losses and is thus expressed as,

$$B = B_0 e^{j(\omega t - \delta)} \quad (3.10.3)$$

where, δ is the phase angle and marks the delay of B with respect to H . The permeability is given by

$$\begin{aligned} \mu &= \frac{B}{H} = \frac{B_0 e^{j(\omega t - \delta)}}{H_0 e^{j\omega t}} \\ &= \frac{B_0}{H_0} \cos\delta - j \frac{B_0}{H_0} \sin\delta \\ &= \mu' - j\mu'' \end{aligned} \quad (3.10.4)$$

$$\text{Where, } \mu' = \frac{B_0}{H_0} \cos\delta \quad (3.10.5)$$

$$\text{and } \mu'' = \frac{B_o}{H_o} \sin \delta \quad (3.10.6)$$

The real part μ' of complex permeability μ as expressed in equation (4.11) represents the component of B, which is in phase with H, so it corresponds to the normal permeability. If there are no losses we should have $\mu = \mu'$. The imaginary part, μ'' corresponds to that part of B, which is delayed by phase angle 90° from H. The presence of such a component requires a supply of energy to maintain the alternating magnetization, regardless of the origin of delay. The ratio of μ'' to μ' gives

$$\frac{\mu''}{\mu'} = \frac{\frac{B_o}{H_o} \sin \delta}{\frac{B_o}{H_o} \cos \delta} = \tan \delta \quad (3.10.7)$$

The $\tan \delta$ is called the Loss Factor. The Q-factor or quality factor defined as the reciprocal of this loss factor, i.e.

$$Q = \frac{1}{\tan \delta} \quad (3.10.8)$$

3.11 Permeability Measurement

The test fixture (16454A) measures core shape magnetic material. The self-inductance of the measurement circuit including MUT is derived as follows:

$$\begin{aligned} L &= \frac{1}{I} \int \mathbf{B} ds \\ L &= \int_a^{d+h_0} \int_0^{h_0} \frac{\mu}{2\pi r} dr dz \\ L &= \frac{\mu_0}{2\pi} \left\{ (\mu_r - 1) h \ln \frac{c}{b} + h_0 \ln \frac{b}{a} \right\} \end{aligned} \quad (3.11.1)$$

After modification of the equation, we get the relative permeability μ_r of MUT (Material Under Test) as:

$$\mu_r = \frac{2\pi L - L_{ss}}{\mu_0 F} + 1 \quad (3.11.2)$$

Where, L_{ss} , is the self-inductance of the fixture when it is empty.

$$L_{ss} = \frac{\mu_0 h_0}{2\pi} \ln \frac{b}{a} \quad (3.11.3)$$

F is the shape function of MUT, which is decided by its dimensions only, hence it is expressed as:

$$F = h \ln \frac{a}{b} \quad (3.11.4)$$

When the magnetic field, generated owing to flow of alternating current, is applied to the magnetic material, the permeability is then the complex permeability and is defined as:

$$\dot{\mu}_r = \mu'_r - j\mu''_r \quad (3.11.5)$$

Where μ'_r is the real part, which is actually for the energy storage and μ''_r is the imaginary part that is the loss factor. Since the inductor has a loss factor, the inductance is modified to complex impedance, which includes the loss:

$$L \rightarrow \frac{\dot{Z}}{j\omega} \quad (3.11.6)$$

The complex relative permeability of the MUT can then be determined by the following equation:

$$\dot{\mu}_r = \frac{2\pi}{\mu_0} \frac{\frac{\dot{Z}}{j\omega} - L_{ss}}{F} + 1 \quad (3.11.7)$$

The schematic diagram of sample holder for the measurement of complex permeability is depicted in figure-3.11[a]. The schematic diagram of Agilent Impedance Analyzer is shown in figure-3.11 [b]

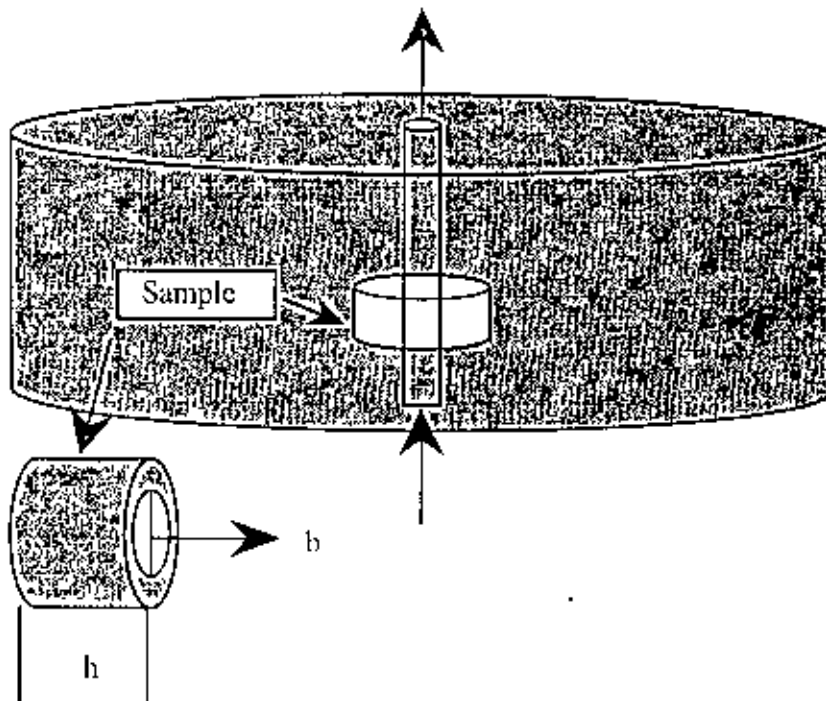


Figure-3.11(a) The schematic diagram of sample holder

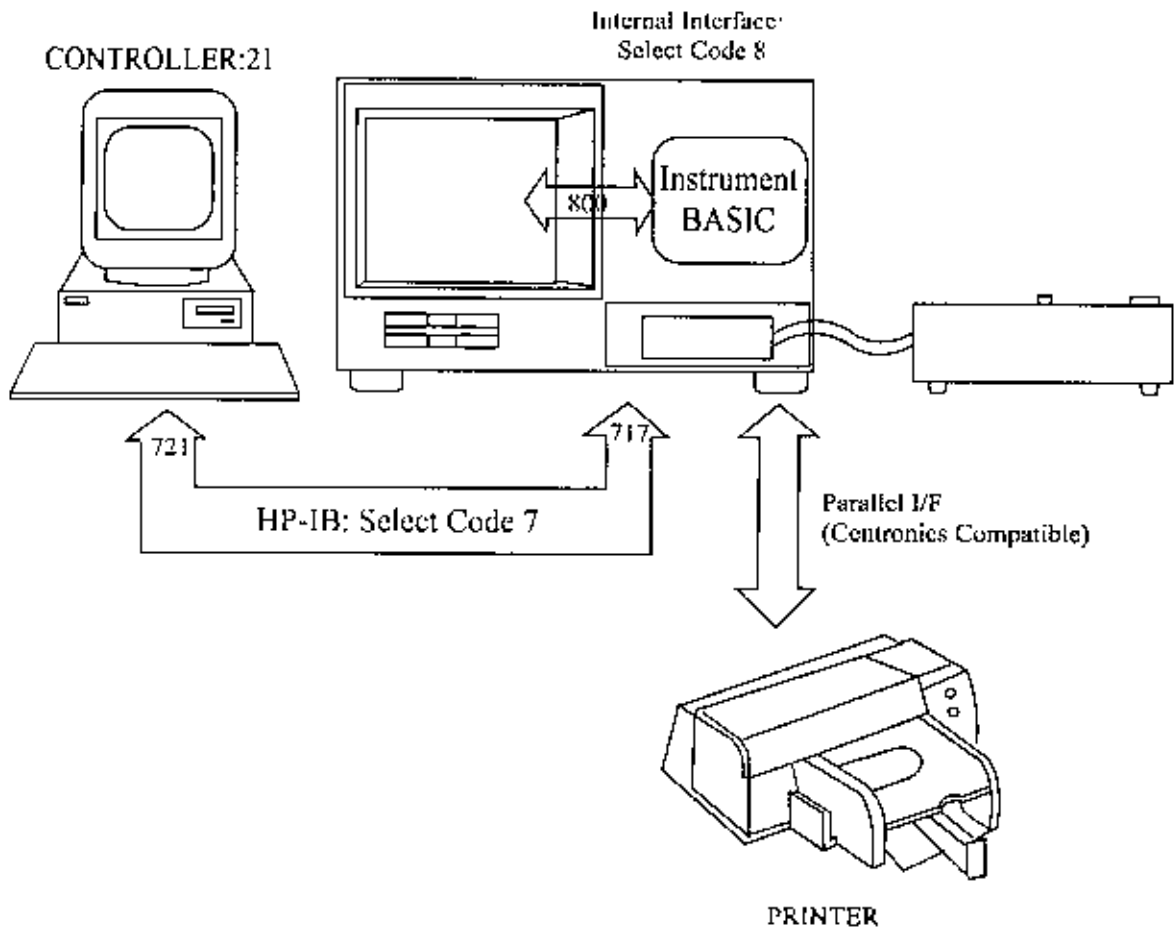


Figure-3.11(b) The schematic diagram of Agilent Impedance Analyzer

Short Brief: Agilent impedance Analyzer has in built enormous provisions to measure the impedance, permeability and permittivity both in room and high temperature range. It can measure the aforesaid parameter in the frequency range 1 MHz ~ 1.5 GHz. Low impedance test head is used to measure permeability and high impedance test head is used to measure the dielectric constants at room temperature. For high temperature similar test heads are available along in-built heating system. Required software is also provided to interface the system with PC for automatic data acquisition.

Chapter-4 RESULTS AND DISCUSSION

4.1. X-ray diffraction

Figure 4.1 shows the X-ray diffraction of as cast sample. The figure shows the amorphous structure of the sample over the scanned angular range from 3° to 70° .

Figure shows the X ray diffraction of the us prepared $Fe_{73}Cu_1Nd_{3.5}Si_{14}B_{8.5}$ sample. The characteristic broad peak at low angle shows the amorphous structure of the sample.

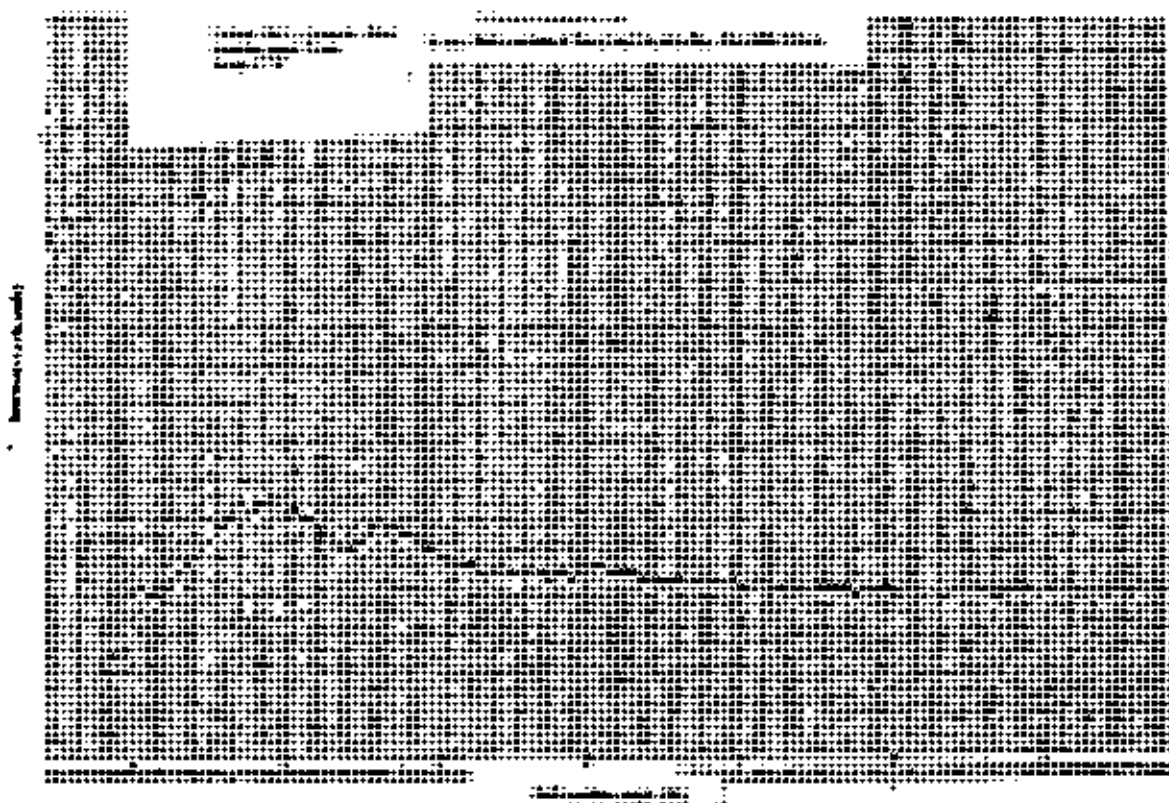


Figure 4.1 X-Ray Diffraction

4.2 Magnetic permeability :

The magnetic permeability of the sample has been measured as a function of frequency in the range 1-10 MHz on as cast and also on the annealed samples

It is observed that in the figure 4.2.1 the as cast sample has an initial permeability orders of magnitude lower than in the kHz Range which is about 3000 at 1 kHz .

The a.c permeability is a measure of magnetic softness. At low frequency the finemet is a very useful alloy to be used as a core material. However, the technological interest does not set any limit on the frequency of its operation. Therefore, at higher frequencies where usually the ferrites are proved to be useful, these alloy system can also be used for certain specific purpose.

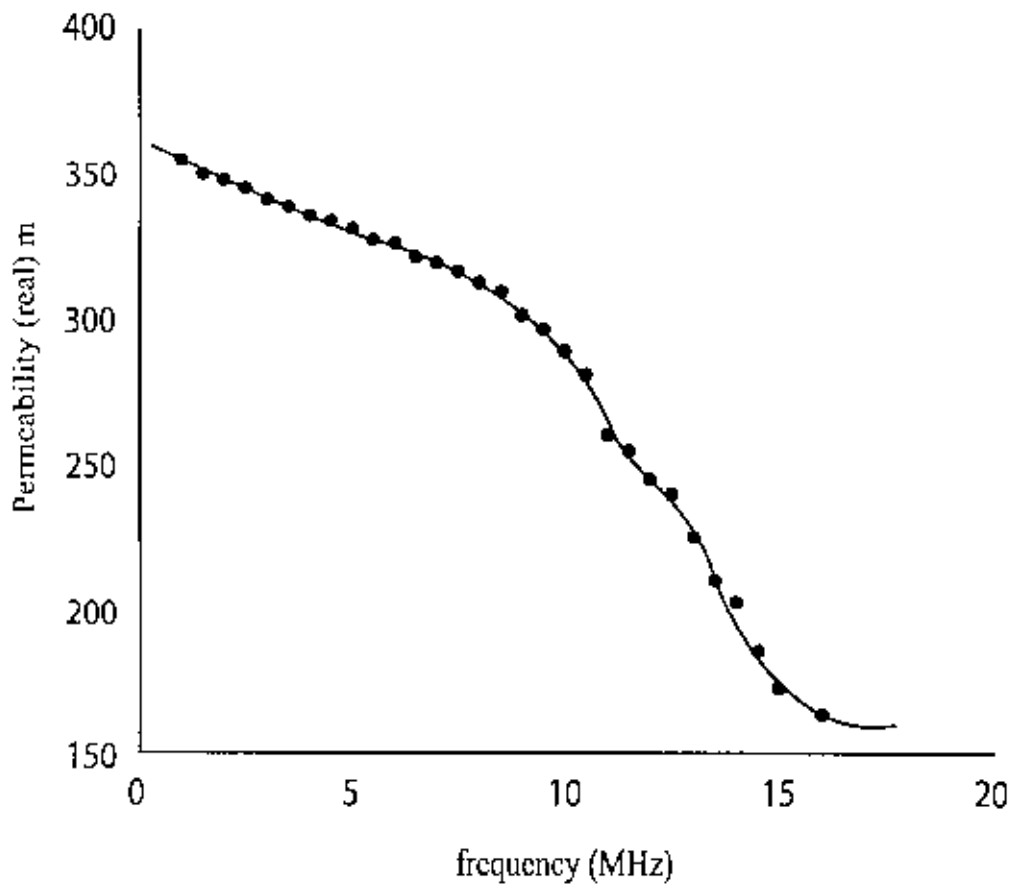
The enhanced permeability values also confirm the reduced magnetic anisotropy due to the formation of nanograins. According to the Random anisotropy model, the critical grain diameter D_{cr} at which the exchange length L_x becomes comparable, the anisotropy drops to few joules/m³ from a scale of 8 kjoule/m³ .

Figure 4.2.2 shows the ac permeability values of as cast and annealed sample. There is a remarkable increase in the permeability. From the non zero values of the permeability and the asymptotically decreasing nature shows that the sample remains magnetically responsive even at higher frequencies.

Figure shows the ac permeability measured on the as cast and also on annealed samples Since controlled annealing induces immediate stress relief on the grains, therefore annealing for a shorter interval around the crystallization temperature T_x causes the formation of nanograins with the enhancement of permeability.

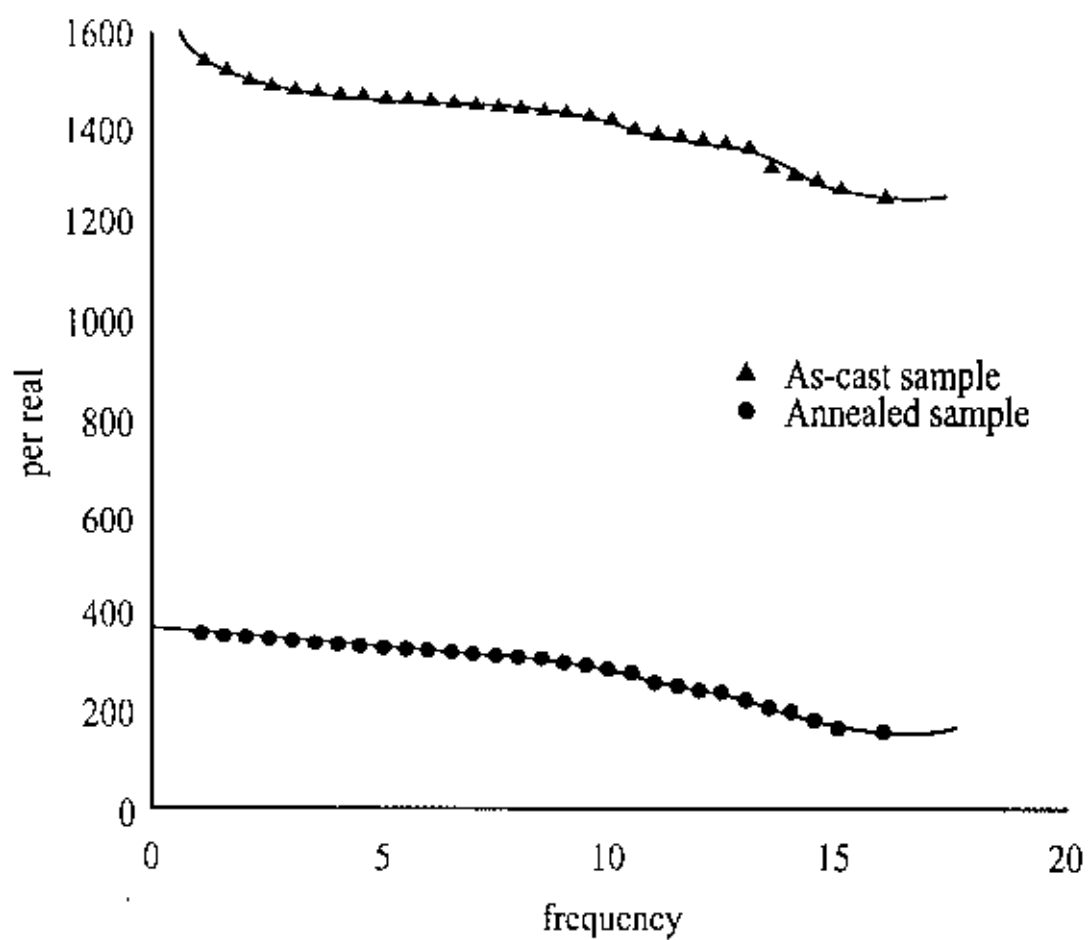
Fig.2 shows the frequency dependence of real part of the a.c. permeability . Usually a low value of the ac permeability (a few hundreds) is obtained around this frequency range. However, a controlled annealing yields a better value of the permeability. This is due to the formation of nano-grains and eventual reduction in the magnetic

anisotropy. At even higher annealing temperatures the permeability increases rapidly due to the structural relaxation.



Frequency Vs Permeability (real)
for As-cast Sample

Figure 4.2.1



Frequency Vs Permeability (real)

Figure 4.2.2

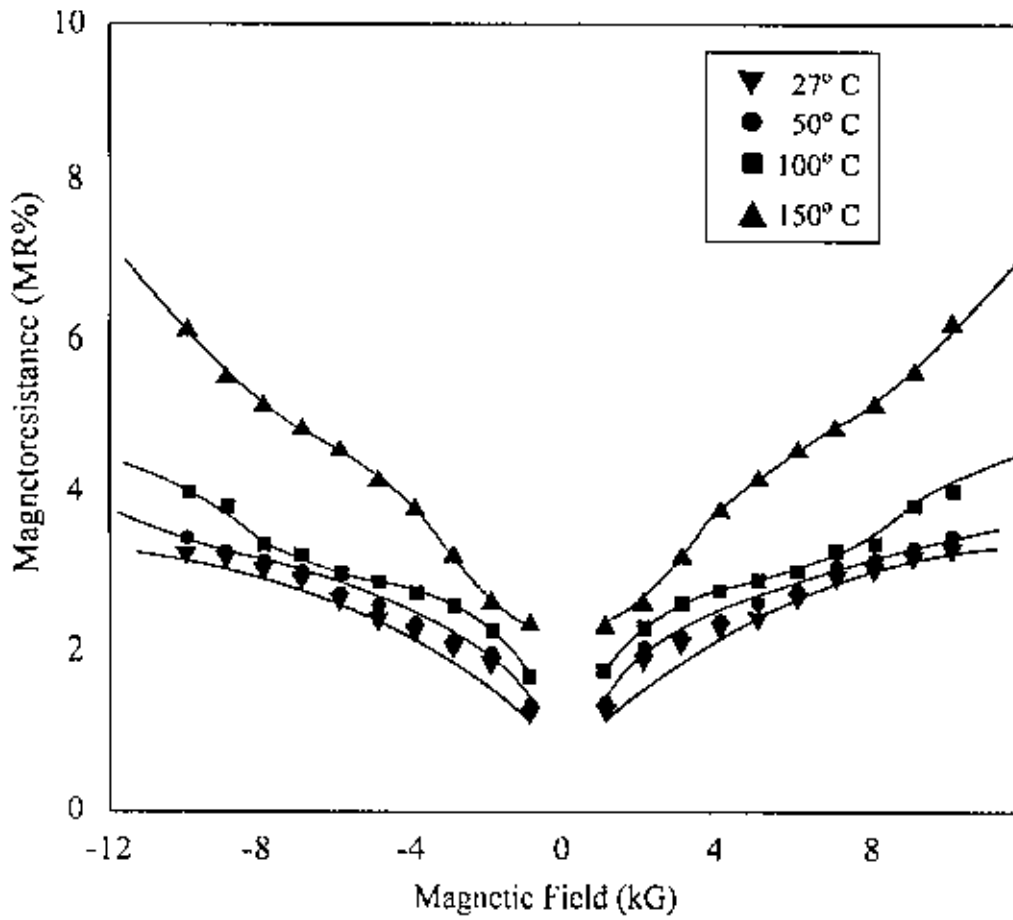
4.3 Temperature dependent Magneto-resistance

The figure 4.3.1 shows the magneto-resistance value is observed to have increased with temperature as a typical nature of these types of Finemets.

The increased value of magneto-resistance is attributed to the presence of spin scattering centers created with the increase of temperature.

The possible electron-phonon scattering is also responsible for the enhanced values of magneto-resistance

Magneto-resistance as a secondary effect is also a parameter which indicates the amount of magnetic crystallites present in the amorphous matrix. Annealing above the crystallization temperature for longer time would give rise to the formation of grain coarsening and the gradual evolution of the non-magnetic boride phase . Fig.4.3.1 shows the magneto-resistance of $Fe_{73}Cu_1Ni_{3.5}Si_{14}B_{8.5}$ as a function of field and temperature. The curves show that the magneto-resistance values increase rapidly at lower magnetic fields , but gradually flattens off at higher fields. This nature of magneto-resistance is typical of Finemet .The magneto-resistance show a gradual decrease as the temperature is increased. This is expected as more and more nano-grains enter into the paramagnetic phase as the temperature is increased. Magneto-resistance which results from the deflection of magnetic ions by the magnetic field will reduce as the temperature is increased. However, a reduction in magneto-resistance is of course expected to influence the electrical resistivity showing an enhancement in electrical resistivity due to the presence of spin scattering centers.



Field dependent magnetoresistance at different temperatures

Figure : 4.3.1

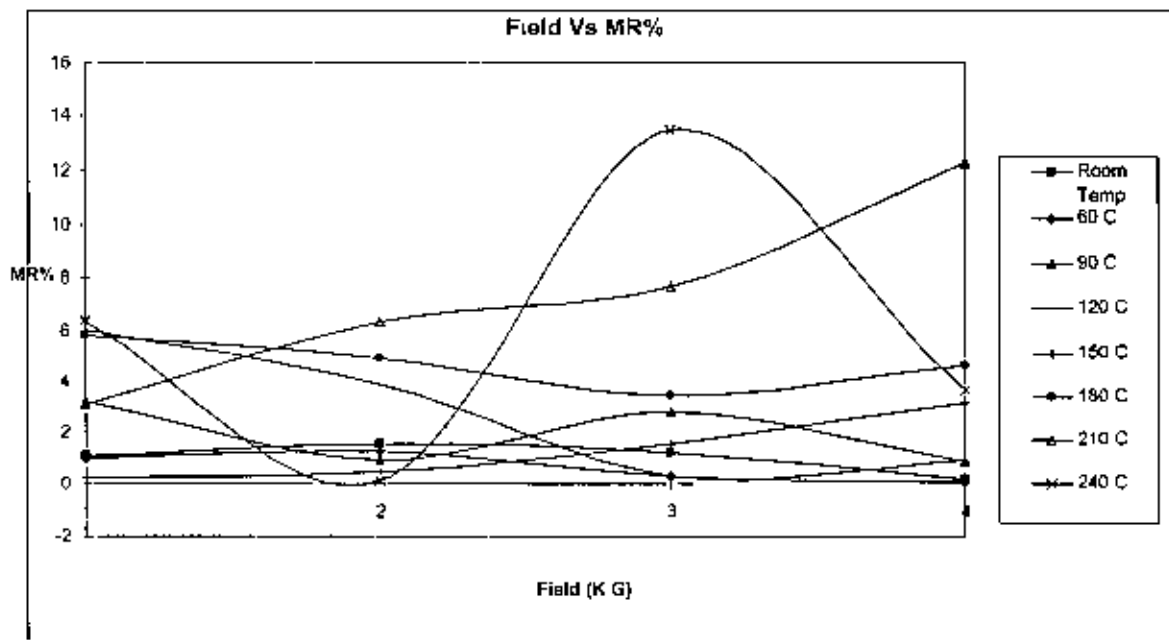
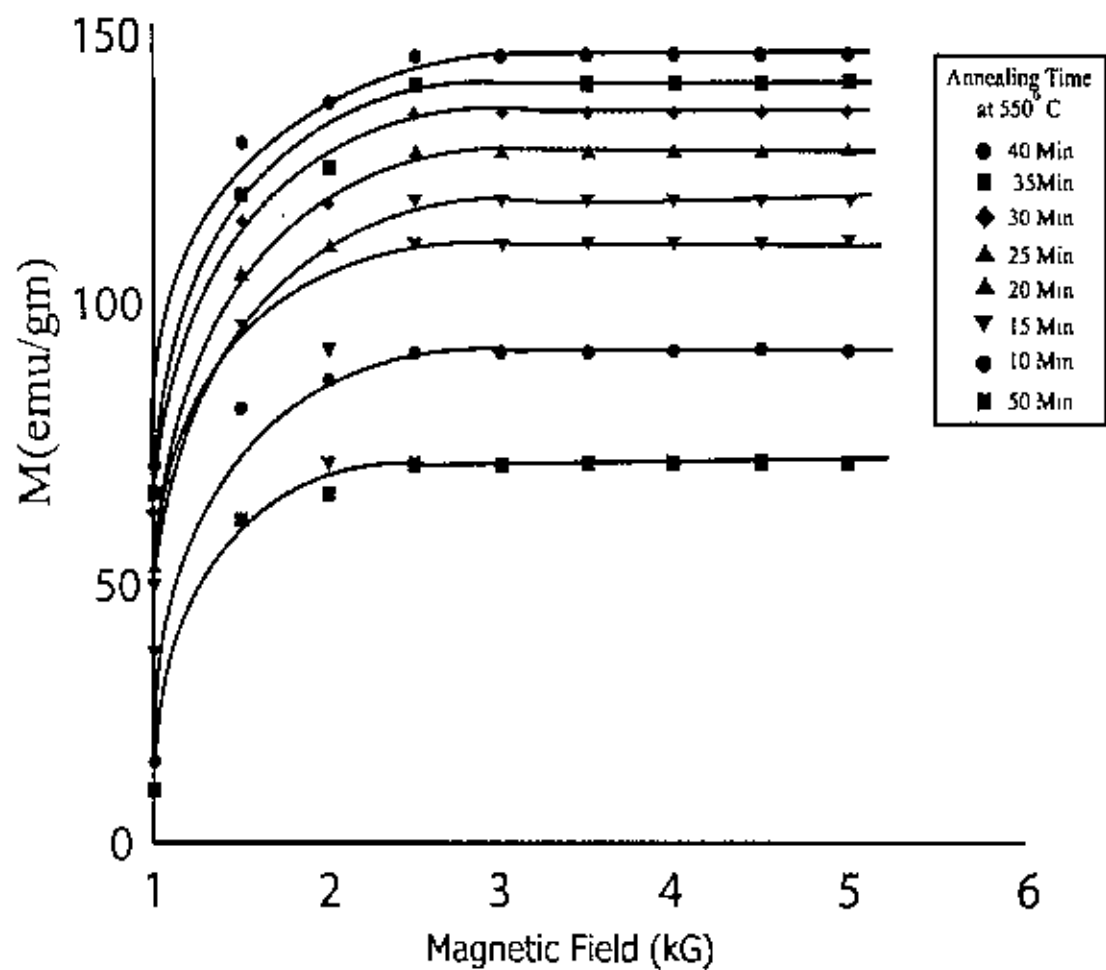


Figure : 4.3.2

4.4 Magnetization Measurements

Figure 4.4 shows Magnetization curves for different annealed samples. The curves show that the magnetization for different samples increases accordingly as their annealing time is increased. The gradual enhancement of magnetization indicates the onset of nanocrystalline structure.

Fig.... Shows the evolution of the microstructure and the soft magnetic properties with annealing temperature. The saturation magnetizations show remarkable enhancements of magnetization upon successive controlled annealing around the crystallization temperature. Annealing near the crystallization temperature for a shorter duration should usually release the mechanical stress created during the growth process. The nanocrystalline state is achieved by annealing the sample at temperatures typically between 500°C and 600°C which leads to primary crystallization of b.c.c iron. The resulting microstructure is characterized by randomly oriented ultra fine grains of b.c.c. Fe-Si with typical grain sizes of 10-15 nanometer embedded in a residual amorphous matrix which occupies 20-30% of the volume and separates the crystallites at a distance 1-2 nm. These features are the basis for the excellent soft magnetic properties indicated by the high values of the initial permeability of about 10^5 and correspondingly low coercivities of less than 1 A/m.



Magnetization curves of Fe₇₃-Cu₁-Nb_{3.5}-Si₁₄-B_{8.5}

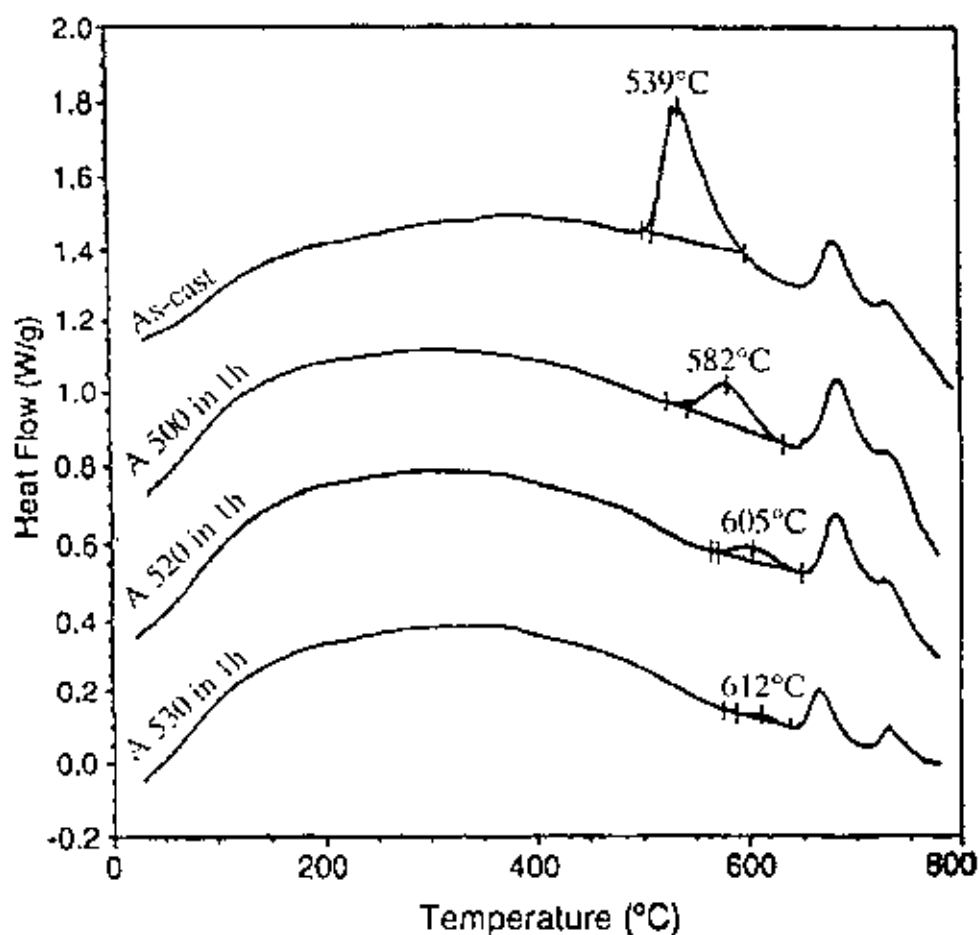
Figure: 4.4

4.5 Differential Scanning Calorimetry (DSC)

The DSC measurements have been done on the different annealed samples. The observed first peak indicates the formation of α -Fe phase of the sample. Around this temperature the process of nano-grains formation starts. The process is usually completed within a narrow temperature window.

It is observed that the peak temperature shifts to the higher values with the increasing of annealed temperature.

The smaller peak at a higher temperature indicates the onset of the formation of boride phase. In this phase the magnetization drops rapidly which is attributed to the grain-coarsening.



Differential Scanning Calorimetry of $\text{Fe}_{73}\text{Cu}_1\text{Nb}_{3.5}\text{Si}_{14}\text{B}_{8.5}$ Metglass
Figure 4.5

4.6 Spin-Glass

The spin-glass behavior is observed on samples with some aging effect.

A typical spin-glass behavior is shown when Mn atoms in an antiferromagnetic system has trace element of Cu atoms as neighbors (Cu-Mn). Similar nature is expected to happen with Fe nanograins have trace element of Cu grains as neighbors (Fe-Cu).

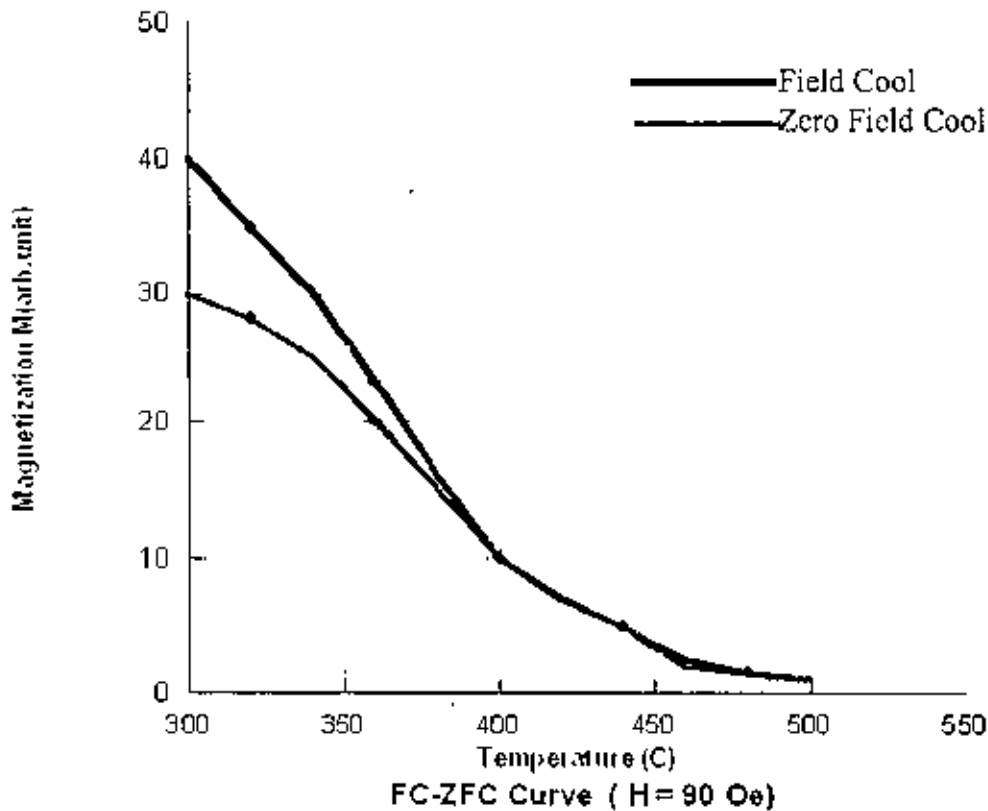


Figure 4.6

Field-cool (FC) and Zero Field Cool (ZFC) measurements have been done to observe some possible relaxation effect. It is observed from these measurements that a small but clear bifurcation has taken place well below the glass transition temperature depicting a spin-glass like behavior. In a FC-ZFC measurement the sample is first heated close to the

glass transition temperature T_g . A small magnetic field about 90 Oe is applied. The sample was then cooled upto the room temperature and the magnetic field was withdrawn. The sample was then heated again upto the same temperature showing a bifurcation around 400 °C .

Chapter-5: CONCLUSION

5.1 CONCLUSION

Since the development of the nanocrystalline $\text{Fe}_{73}\text{Cu}_1\text{Nb}_{3.5}\text{Si}_{14}\text{B}_{8.5}$ alloy many investigations have been performed on this material and in the present work a quantitative investigation on the magneto-transport properties of this alloy have been performed. The as cast and annealed samples have shown remarkable differences in the transport properties. The as cast sample in the amorphous state has a Curie temperature much below the crystallization temperature. However, a controlled annealing process around T_x takes the T_c to a much higher value.

In the X-ray diffraction the broad peak represents the amorphous structure of the alloy and in this alloy the presence of Nb stabilizes the amorphous structure and impedes the formation of the corresponding crystalline boride compounds.

A controlled annealing of the sample around the crystallization temperature gives rise to the formation of nanograins. Only annealing at more elevated temperatures above 600°C leads to the precipitation of small fractions of boride compounds like Fe_2B or Fe_3B with typical dimensions of 50nm to 100nm, while the ultrafine grain structure of b.c.c. Fe-Si still persists. Further increase of the annealing temperature above about 700°C finally yields grain coarsening. Both the formation of the borides and grain coarsening deteriorates the soft magnetic properties significantly. The annealed time should not be for several hours and it was found that a typical heat treatment for 1h at 540°C in most cases yields a nanocrystalline microstructure close to the quasi-equilibrium state and characteristics for the individual alloy composition.

The magnetoresistance values have shown a significant variation with the increase of measuring temperature. A significant permeability values were obtained at higher frequency range (MHz) for as-cast sample and annealed sample and the permeability decreases monotonically as the frequency is increased. In the low frequency range the permeability is of the order of 10^5 . A controlled annealed sample for a shorter time

duration around the glass transition temperature T_g gives rise to a larger value of permeability than the as-cast sample and both the samples show a good response in lower frequencies as well as high frequencies.

The relaxation effect which is typical for a spin glass has been observed through FC and ZFC measurements depicting some degree of irreversibility. Relaxation effect has been observed in previous works (K. Gunnarsson 1991) between Cu and Mn with Mn being an antiferromagnetic element in the neighborhood of Cu. In the $Fe_{73}Cu_1Nb_3Si_{14}B_{8.5}$ system there may be some kind of coupling between Fe and Cu when the amorphous matrix is transformed into nanocrystalline phase.

The formation of nano-crystalline structure is confirmed by DSC measurements through the observation of the peak where first one represents the α -Fe(Si) phase and later the boride phase.

5.2 Suggestions for future work:

Nanocrystalline Fe based alloys having the combination of high saturation magnetization, high permeability, good frequency response, low losses and the good thermal stability gives the scope for further research.

Permeability which is measured at room temperature in the present work can be examined at various temperatures with the Agilent impedance analyzer. There is an opportunity to measure the temperature response of complex permeability, permittivity and impedance of Nanocrystalline Fe based alloys. Moreover the magnetostriction, coercivity and magnetic anisotropy for this type of material are proposed for further research work.

Bibliography

- 1 Y. Yoshizawa, S. Oguma, and K. Yamauchi, "New Fe-based Soft Magnetic Alloys Composed of ULTRAFINE Grains Structure", *J. Appl. Phys.* 64, p6044 (1988).
- 2 Y. Yoshizawa, K. Yamauchi, T. Yamane, and H. Sugihara, *J. Appl. Phys.* 64, p 6047 (1988).
- 3 G. Herzer, *IEEE Trans. Mag.* 25 2227 (1989).
- 4 G. Herzer, "Grain size dependence of coercivity and permeability in nanocrystalline" *IEEE Trans. Mag.* 26 1379 (1990).
- 5 G. Herzer, "Grain structure and magnetism of nanocrystalline ferromagnets" *IEEE Trans. Magn* 25 (1989) 3327.
- 6 Y. Yoshizawa and K. Yamauchi, *Mater. Sci. Eng.* A133 (1991) 176.
- 7 P. Duhaj, P. Zvee. D. Janickovie and I. Matko, *Mater. Sci. Eng.* A133 (1991) 395.
- 8 T. Kulik, *Mater. Sci. Eng.* A159 (1992) 95.
- 9 G. Herzer, *Mater. Sci. Eng.* A133 (1991) 1.
- 10 R. Zuberek, M. Batan, T. Kulik and H. Szymczak, *Proc. Int. Conf. Physics of Transition metals.* eds. P. M. Oppinger and J. Qubler (World Scientific, Singapore, 1993) Vol.2. P.946.
- 11 T. Kulik, R. Zuberek and A. Hernando, *J. Magn. Magn. Mater.*
- 12 M. Bazqez, P. Marin. A. Olofinjana and H. A. Davies, *J. Magn. Magn. Mater.* To be published.
- 13 G. Herzer, *Proc. Int. Symp. On 3rd Transition Semi Metal Thin Films, Sendal, 1991,* P.136.
- 14 M. Muller, N. Mattern, I. Ilgen, *Z. Metallkde* 82 (1991) 895.
- 15 G. Hampel, A. Pundt and J. Hesse, *J. Phys. Condensed Matter* 4 (1992) 3195.
- 16 Y. Yoshizawa and K. Yamauchi, *IEEE Trans. J. Magn. Jpn.* , 5 (1990) 530.
- 17 G. Herzer, *Phys. Scr* , T49 (1993) 307.
- 18 K. Twarowski, M. Kuźmiński, A. Ślawska-Waniewska, H. K. Lachowicz and G. Herzer, *J. Magn. Magn. Mater.* 150 (1995) 85.
- 19 A. Ślawska-Waniewska, M. Gutowski, N. Kuźmiński, E. Dynowska and H. K. Lachowicz, G. C. Hadjipanayis and R. W. Siegel, (eds.) , *Nanophase Material*, Kluwer, Dordrecht, 1994, P.721.
- 20 E. Jedryka, N. Randrianantoandro, J. M. Grenéche. A. Ślawska-Waniewska, H. K. Lachowicz, *J. Magn. Magn. Mater.*, 140-144 (1995) 451.
- 21 A. Ślawska-Waniewska, M. Gutowski, H. K. Lachowicz, T. Kulik and H. Matija,

- Phys. Rev. B*, 46 (1992) 14 594.
- 22 H. Barkhausen, *Phys. Z.*, 20 (1919) 401.
 - 23 B. Alesandro, C. Beatris, G. Bertotti and A. Montorsi, *J. Appl Phys.*, 64 (10) (1998) 5355.
 - 24 Y. Yoshizawa, S. Oguma, and K. Yamauchi, "New Fe-based Soft Magnetic Alloys Composed of ULTRAFINE Grains Structure", *J. Appl. Phys.* 64, p6044 (1988).
 - 25 T.H Noh, M.BLee, H.J.kim and LK Kang , "Relation between crystallization process and magnetic properties of Fe-(Cu-Nb)-Si-B amorphous alloy", *J. Appl. Phy.vol.67p5568(1990)*
 - 26 Y. Yoshizawa and K. Yamauchi, *IEEE Trans.J Mag.* vol.5p.1070(1990b)
 - 27 M.Muller, and N Matern, "The influence of refractory element additions n the magnetic properties and on the crystallization behavior of nano crystalline soft magnetic Fe-B-Si_Cu alloys", , *J. Mag. Mag. Mater.*, vol.136,p.79(1994)
 - 28 R. Alben, J.J Becker and M.C.Chi, "Random Anisotropy in amorphous ferromagnets", *J. Appl. Phy.vol.49,p.1653(1978)*
 - 29 T.Sawa. and Y.Takahashi, " Magnetic properties of FeCu (3d transition metals) Si B aloys with fine grain structure", *J. Appl. Phy.vol.67,p.5565(1990)*
 - 30 K. Sujuki, A.Makino, N.Kataoka, A Inoue and T. Masumoto, "Soft magnetic properties of nano-crystalline bcc Fe-Zr-B-Cu (M=transition metal) alloys with high saturation magnetization" *J. Appl. Phy.vol.70,p.6232(1991)*
 - 31 K. Hono, A. Inoue and T. Sakurai,*Appl. Phys. Lett.* 58, 2180 (1991).
 - 32 K. Hono, K. Hiraga, Q. Wang, A. Inoue and T. Sakurai, *Acta. metall. mater.* 40, 2137 (1992).
 - 33 K. Hono, J.-L. Li, Y. Ueki, A. Inoue and T. Sakurai, *Appl. Surf. Sci.* 67, 398 (1993).
 - 34 K. Hono, Y. Zhang, A. Inoue and T. Sakurai, *Mater. Trans. JIM*, 36, 909 (1995).
 - 35 D.Frunball, *J. de Physique*, vol.35, C4-1(1974)
 - 36 H.K.Lachowic,A. Slawska-Waniewska,"Co-existence of various mgnetic phases in nanocrystalline Fe- based metallic glasses" , *J. Mang. Matter.* Vol.133,p.238(1994)
 - 37 S.Takayama, *J. Material Sci.*vol.11, p.164 (1976)
 - 38 G.Herzer, *Handbook of Mag.Matter*, vol.10, p.437(1997)
 - 39 A.E. Berkowitz, J.L. Walter and K.F. Wall,"magnetic Properties of Amorphous particles Produced by Spark Erosion", *Physs. Rev. Lett.* vol.46, p.1484(1981)
 - 40 W. Thomson, *Proc. Roy. Soc.(London)*8,546(1851),*Phil.Mag.IV*,15,469(1858)
 - 41 N.F. Mott,"Elcctrons in Transition Metals", *Proc. Roy. Soc.(London)*,vol. A156, p.368 (1936)
 - 42 T. Kasua, *Magnetism-11B*, Academic Press,p.215(1966)
 - 43 Duwez, *IEEE Trans. Magn*, vol.26,p.1397,(1990)
 - 44 S. Edwards and P. Anderson, *J. Phys. F* 5, 965(1975)
 - 45 K H Fisher and J. A. Hertz, in "Spin Glasses", edited by D Edwards and D. Melville(Cambridge University Press, Cambridge 1991).

- 46 D.S. Fisher, G. M. Grinstein, and A. Khurana , *Physics today* 41, 56 (1988)
- 47 P. Norblad and P. svedindh, in "Spin Glasses and Random Fields" , edited by A.P. Young (World scientific publishing Co, Singapore,1988)
- 48 K. Binder and A.P. Young, *Rev. Mod. Phys.* 58, 801(1986)
- 49 W.L. McMillan, *Phys. Rev. B* 31, 342(1985); J.A. Olive, A.P. young, and A.P. Sherrington, *Phys. Rev. B* 34,6431(1986); B.M. Morris, S.G. Colborne, M.A. Moore, A.J. Bray, and J. Canisius, *J.Phys. C* 19, 1157(1986); Y. Ozeki, and H. Nishimura, *J phys. Soc. Jpn.* 57,4255(1988)
- 50 H. Kawamura and M Tanemura. *J. Phys. Soc Jpn.* 54,4479(1985)
- 51 A.J. Bray, M.A Moore, and A.P. Young, *Phys. Rev. Lett.* 56,2641(1986)
- 52 M. Rudderman and c. Kittel, *Phys Rev.* 96, 99 (1954); T. Kasuya, *Prog. Theor. Phys.(Kyoto)* 16,45 (1956); K. Yosida , *Phys. Rev.* 106,893 (1957).
- 53 H. Aruga and A. Ito, *J. Phys. Soc. Jpn.* 62,4488(1993)
- 54 A. Ito, H. Aruga, M. Kikuchi, YSyono and H. Takei, *Solid state Commun.* 66,475 (1988); A. Ito, H. Aruga, E. Torikai, M. Kikuchi, YSyono and H. Takei, *Phys. Rev.Lett.* 57,483 (1986)

Table: 1
Measurement of Temperature Dependent Magnetoresistance at
Different Filed

Field (KG)	MR% at 27°C	MR% at 50°C	MR% at 100°C	MR% at 150°C
1	1.2	1.3	1.7	2.3
2	1.8	1.95	2.2	2.58
3	2	2.1	2.5	3.15
4	2.2	2.3	2.65	3.75
5	2.3	2.5	2.78	4.15
6	2.6	2.65	2.9	4.55
7	2.8	2.95	3.15	4.85
8	2.9	3.05	3.26	5.15
9	3.1	3.2	3.75	5.55
10	3.15	3.35	3.95	6.15
-1	1.2	1.3	1.7	2.3
-2	1.8	1.95	2.2	2.56
-3	2	2.1	2.5	3.15
-4	2.2	2.3	2.65	3.75
-5	2.3	2.5	2.78	4.15
-6	2.6	2.65	2.9	4.55
-7	2.8	2.95	3.15	4.85
-8	2.9	3.05	3.26	5.15
-9	3.1	3.2	3.75	5.55
-10	3.15	3.35	3.95	6.15

Table: 2
Measurement of Temperature Dependent Magnetoresistance for Field Cool and Zero Field Cool

Temperature (°C)	MR% for Field Cool	MR% for Zero Field Cool
300	30	40
320	28	35
340	25	30
360	20	23
380	15	16
400	10	10
420	7	7
440	5	5
460	2	2
480	1.5	1.5
500	1	1

Table:3
I-V Measurement for Different Field at 27⁰C

Current (mA)	Voltage in mV				
	0 (KG)	4 (KG)	3.12 (KG)	2.03 (KG)	0.99 (KG)
0	1.947	1.988	2.002	1.996	1.866
10	5.251	5.288	5.831	6.806	6.399
20	10.089	9.506	10.403	13.192	9.218
30	13.701	14.994	13.765	16.602	15.75
40	18.997	18.853	20.108	20.486	19.649
50	23.331	23.426	24.004	23.672	24.251
60	29.045	28.799	28.225	29.141	28.295
70	34.66	34.107	32.54	33.92	32.542
80	38.324	38.05	39.537	40.288	38.552
90	42.276	43.707	43.409	43.805	43.355
100	46.322	46.533	47.48	48.062	47.698
110	51.435	51.637	51.718	51.94	51.655
120	55.499	55.701	56.137	56.016	57.474
130	62.368	60.642	60.906	60.611	62.313
140	66.61	65.585	66.03	66.101	67.032
150	69.438	69.296	70.62	69.638	70.75
160	75.615	74.947	75.392	74.251	75.706
170	79.5	79.555	80.515	80.426	79.795
180	83.918	83.57	85.983	85.902	84.377
190	88.331	88.532	89.341	90.665	89.17
200	92.226	93.137	95.541	95.969	94.385

Table: 4
I-V Measurement for Different Field at 60°C

Current (mA)	Voltage in mV				
	0 (KG)	4 (KG)	3.12 (KG)	2.03 (KG)	0.99 (KG)
0	2.085	1.921	2.114	2.123	2.135
10	6.106	5.531	7.037	7.592	6.509
20	11.378	9.53	10.699	12.234	11.089
30	15.908	15.63	15.819	16.451	14.943
40	20.661	19.604	21.13	20.109	19.861
50	25.234	24.72	26.086	24.293	24.423
60	29.124	29.098	30.671	28.309	28.546
70	33.979	34.587	34.704	33.552	37.551
80	39.12	39.724	38.99	38.592	42.237
90	44.617	44.295	43.325	45.543	46.765
100	49.551	49.236	48.354	50.162	50.615
110	55.037	55.63	54.686	56.975	55.209
120	60.33	61.677	60.374	60.043	58.89
130	64.545	64.773	63.681	65.375	63.107
140	68.39	68.819	69.198	69.425	69.737
150	72.048	73.577	72.127	75.837	74.532
160	76.808	77.053	76.904	79.517	80.254
170	83.387	81.637	81.501	83.754	83.565
180	87.3958	87.861	88.344	88.167	88.173
190	92.53	91.518	94.184	92.376	92.43
200	98.252	97.403	99.501	98.628	96.999

Table: 5
I-V Measurement for Different Field at 90°C

Current (mA)	Voltage in mV				
	0 (KG)	4 (KG)	3.12 (KG)	2.03 (KG)	0.99 (KG)
0	2.251	2.067	2.264	2.287	2.277
10	6.25	8.013	5.707	7.099	6.699
20	10.704	12.731	11.319	10.979	10.225
30	15.92	19.049	17.34	16.039	15.325
40	19.877	22.72	23.941	20.712	21.161
50	25.621	26.423	29.982	25.209	26.266
60	31.036	31.064	37.545	30.85	32.709
70	36.837	37.084	41.436	36.095	38.245
80	41.864	42.503	48.054	42.72	44.446
90	46.314	47.144	53.667	47.986	48.982
100	51.728	52.769	57.357	52.286	52.87
110	55.62	57.608	57.565	56.58	58.936
120	61.596	63.239	64.187	61.675	63.629
130	67.015	67.716	69.061	68.098	69.892
140	72.636	72.571	73.538	73.554	73.24
150	77.304	76.665	77.995	78.448	77.76
160	81.71	82.095	83.265	84.324	83.837
170	87.191	86.754	88.333	89.022	91.293
180	92.635	93.382	91.86	92.538	96.585
190	97.302	98.823	97.314	97.426	100.912
200	103.499	103.111	103.346	102.522	105.221

10/5/2013

Table: 6
I-V Measurement for Different Field at 120°C

Current (mA)	Voltage in mV				
	0 (KG)	4 (KG)	3.12 (KG)	2.03 (KG0)	0.99 (KG)
0	2.371	2.355	2.368	2.396	2.392
10	6.559	7.177	7.207	8.468	7.415
20	12.196	11.228	12.1	13.156	11.57
30	17.858	16.276	17.179	18.068	16.514
40	23.499	22.348	21.069	22.602	21.14
50	28.738	28.228	26.739	29.121	28.846
60	34.211	34.157	31.205	34.659	33.951
70	39.661	38.974	35.503	39.974	40.559
80	44.122	43.894	40.386	47.572	46.126
90	48.572	49.745	45.878	52.288	50.832
100	53.45	54.592	50.772	58.437	56.821
110	59.089	60.058	55.881	62.397	63.128
120	64.565	65.159	61.626	67.49	68.115
130	69.438	69.431	66.889	72.846	74.079
140	73.904	74.111	71.778	78.387	81.295
150	78.755	79.806	81.004	83.509	88.311
160	85.681	86.54	87.334	86.602	95.739
170	90.12	93.644	93.653	91.439	94.128
180	96.216	97.336	98.788	97.706	99.132
190	100.681	101.435	104.5	105.514	105.702
200	107.163	106.62	107.169	110.677	111.855

Table: 7
I-V Measurement for Different Field at 150°C

Current (mA)	Voltage in mV				
	0 (KG)	4 (KG)	3.12 (KG)	2.03 (KG)	0.99 (KG)
0	2.527	2.534	2.56	2.4	2.56
10	8.28	9.183	7.538	8.232	9.813
20	13.215	10.915	12.816	13.065	13.587
30	17.713	18.965	19.594	18.776	18.644
40	22.865	25.024	23.864	24.509	25.066
50	29.764	30.047	29.023	32.659	31.497
60	36.013	35.92	36.933	37.081	36.788
70	42.903	42.44	43.277	43.02	41.015
80	50.228	48.162	49.194	48.526	46.967
90	57.348	52.506	54.582	56.239	55.698
100	63.811	59.712	58.21	62.422	61.829
110	68.989	63.863	63.685	67.924	67.789
120	72.895	69.099	69.63	72.349	73.128
130	80.025	75.004	75.357	77.663	79.58
140	86.318	80.906	81.45	82.218	85.354
150	91.955	86.14	86.787	89.62	91.396
160	99.083	91.843	92.539	94.049	95.335
170	102.565	98.874	97.858	101.799	98.926
180	102.945	103.684	105.578	107.569	106.253
190	108.202	108.773	114.396	114.433	111.357
200	113.695	115.369	120.588	119.357	116.259

Table: 8
I-V Measurement for Different Field at 180°C

Current (mA)	Voltage in mV				
	0 (KG)	4 (KG)	3.12 (KG)	2.03 (KG)	0.99 (KG)
0	2.748	2.558	2.825	2.886	2.646
10	8.559	8.243	7.635	7.759	9.931
20	13.11	13.996	13.965	13.415	16.533
30	19.651	19.982	19.651	18.363	20.35
40	26.146	26.232	25.913	27.731	26.093
50	32.336	32.009	32.608	34.406	33.858
60	37.568	38.766	39.072	41.34	39.408
70	44.944	46.923	45.952	47.785	47.426
80	52.14	52.92	55.047	54.213	54.71
90	56.483	59.427	62.654	59.46	61.482
100	62.196	68.091	69.78	65.167	68.294
110	70.093	74.187	75.214	71.242	74.113
120	76.783	81.166	79.647	79.854	79.637
130	84.444	89.892	85.065	87.08	86.454
140	89.974	97.4	92.197	93.055	93.28
150	95.969	105.198	98.378	99.866	101.18
160	101.086	110.097	106.042	107.853	108.752
170	106.648	116.217	110.514	112.137	114.575
180	114.141	116.415	116.772	120.439	121.483
190	121.425	120.385	122.251	128.021	127.835
200	127.706	127.507	130.942	135.071	135.054

Table: 9
I-V Measurement for Different Field at 210°C

Current (mA)	Voltage in mV				
	0 (KG)	4 (KG)	3.12 (KG)	2.03 (KG)	0.99 (KG)
0	3.598	3.698	3.845	3.642	3.739
10	10.907	11.568	12.726	13.012	12.331
20	18.748	19.021	20.625	22.149	22.458
30	27.665	26.889	27.252	30.891	30.885
40	39.66	33.588	38.485	37.685	40.57
50	46.714	42.551	47.743	49.198	47.956
60	57.864	51.579	54.715	58.163	57.1
70	67.59	60.348	65.006	64.851	67.228
80	76.271	68.14	71.019	73.851	77.619
90	88.138	75.471	86.987	81.825	89.081
100	101.94	85.913	93.719	91.041	99.352
110	108.502	94.737	104.789	101.652	108.546
120	120.131	103.901	109.368	118.902	109.728
130	131.545	111.915	119.146	122.914	122.126
140	145.901	120.775	127.732	128.992	131.72
150	142.57	129.459	137.605	138.484	141.709
160	154.446	138.717	147.229	145.835	153.887
170	164.693	147.861	150.866	154.051	162.639
180	177.658	157.422	163.731	165.035	173.332
190	191.812	167.225	172.715	174.325	176.195
200	199.42	175.129	179.64	187.359	190.298

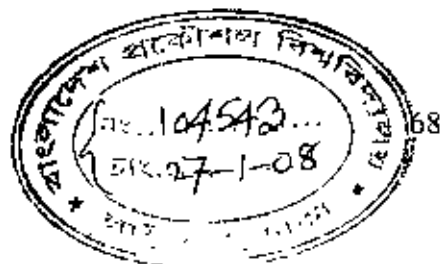


Table: 10
I-V Measurement for Different Field at 240°C

Current (mA)	Voltage in (mV)				
	0 (KG)	4 (KG)	3.12 (KG)	2.03 (KG)	0.99 (KG)
0	4.195	6.32	7.292	5.902	6.305
10	14.365	20.191	24.651	20.797	18.714
20	25.248	35.771	44.199	35.775	29.132
30	33.943	46.135	59.749	47.135	42.765
40	48.427	58.018	79.466	62.389	58.124
50	64.559	76.05	96.652	78.052	76.221
60	82.449	92.504	115.442	91.167	94.925
70	93.748	111.844	135.305	108.258	112.157
80	105.926	124.399	142.811	122.301	125.079
90	118.251	141.288	177.862	137.98	141.427
100	130.641	148.433	196.626	152.883	149.728
110	145.189	164.566	207.649	168.466	169.8
120	162.586	185.115	226.48	188.702	187.599
130	180.702	197.626	239.55	196.896	203.255
140	216.993	219.054	248	207.384	219.71
150	237	237.63	252	223.6	249.62
160	240.9	252.53	271	238.12	257
170	260.77	264.06	330	259.88	272.56
180	305.7	275.7	273.4	268.22	283.5
190	335.3	293.03	298.59	287.7	295.78
200	289.3	335.3	292.3	295.95	355.58

Table: 11
Measurement of Temperature Dependent Magnetoresistance at Different Filed

Field (KG)	MR%. at 27°C	MR%. at 60°C	MR%. at 90°C	MR%. at 120°C.	MR%. at 150°C	MR%. at 180°C	MR%. at 210°C	MR%. at 240°C
0.99	1.0657	0.9595	3.205	6.034	0.2172	5.808	3.07	6.368
2.03	1.495	1.204	0.8937	3.885	0.4344	4.927	6.337	0.0791
3.12	1.174	0.265	2.767	0.2802	1.52	3.434	7.701	13.47
4	0.1285	0.0612	0.8548	0.8966	3.175	4.64	12.25	3.662